Appendix A - Model attributes and methods

An appendix to the report:

Deltares, 2021. Demonstration of the updated Bays Eutrophication Model. Boston: Massachusetts Water Resources Authority. Report 2021-02. 138 p. plus appendices. https://www.mwra.com/media/file/demonstration-updated-bays-eutrophication-model-2021-02

Contents

List of Figures

List of Tables

A.1 Introduction

A.1.1 About this appendix

This appendix describes the model attributes and modeling methods of the updated Bays Eutrophication Model (BEM). It describes the initial model set-up, including aspects such as grid, bathymetry and coastline; water quality model configuration; outfall; river inputs; air-sea interface; offshore boundaries and other relevant model features.

The hydrodynamic equations are described in Appendix A1 and the water quality equations are given in Appendix A2.

The updated BEM has been used for a simulation for 2016 as presented in the main report. The description of the model attributes and modeling methods includes all modifications to the initial model set-up that were made during the multi-year calibration process, which is described in Appendix B.

A.1.2 Modeling platform

The updated BEM has been set-up using the Delft3D-Flexible Mesh (Delft3D FM) Suite software. The software is open source. Delft3D FM Suite can simulate storm surges, hurricanes, tsunamis, detailed flows and water levels, waves, sediment transport and morphology, water quality and ecology, and is capable of handling the interactions between these processes. For the updated BEM, the integrated hydrodynamic and water quality modules of Delft3D FM have been configured for the application to Mass Bay.

A.2 Grid, bathymetry, and coastline

A.2.1 Grid domain and resolution

The model grid is one domain covering the entire Gulf of Maine region as well as the coastal region to the south, down to and including Chesapeake Bay. The model is extended to the South (down to Roanoke Island, North Carolina) to set the grid corner on land, which was required for model stability. To the North, the model extent is similar to the regional Gulf of Maine (GoM) model (GOM4-FVCOM) previously used to nest the local Bays Eutrophication Model (BEM) water quality component (Zhao et al. 2017). The model grid configuration is shown in Figure A.2-1.

In general, the grid has coarser grid cells near the open boundaries and in deep waters, while the resolution increases toward the area of interest and to shallower waters. The advantage of applying a coarse resolution in deep areas in particular is twofold: it reduces the number of cells in areas where allowed by local spatial scales and increases the maximum allowed numerical time step. The grid comprises mostly rectangular grid cells with a number of transition zones between areas of different resolution. Transition zones are created using triangular grid cells.

The horizontal resolution is roughly 8km at the open ocean and is gradually refined towards the coast, with refinement transitions approximately following the 400m, 100m and 50m isobaths for the 4km, 2km and 1km resolution refinements, respectively. In order to further reduce computational times, the resolution away from the area of interest is limited to a maximum of 2km. The 1km resolution is applied only south of the St. John River (border with New Brunswick, Canada) and north of New York City.

An additional refinement level of 0.5km is included for most of the Massachusetts Bay and Cape Cod Bay area as well as a thin coastal strip further north up to Portland Maine. This region of 0.5km resolution extends slightly east of Cape Cod, with a southernmost point at Monomoy Island. Finally, a 250m horizontal refinement level has been introduced in Boston harbor and the surrounding coastline. The MWRA outfall is located in this region with 250m resolution. An overview of the coverage of each resolution is provided in Figure A.2-2.

A z-sigma-layer approach is used for the vertical schematization of the model. This implies that strictly horizontal layers are used, except near the surface where sigma-layers are applied. The thickness of these sigma-layers varies in time according to local variations in water level, while the thickness relative to the local water depth stays the same. The upper 16 layers are initialized with a 2.5 m thickness and treated as sigma-layers during the computation. Below 40 m deep are z-layers with thickness gradually increasing from 2.5 m with each subsequent layer being 18% thicker. This results in a maximum number of layers of 50 in the deepest part of the model.

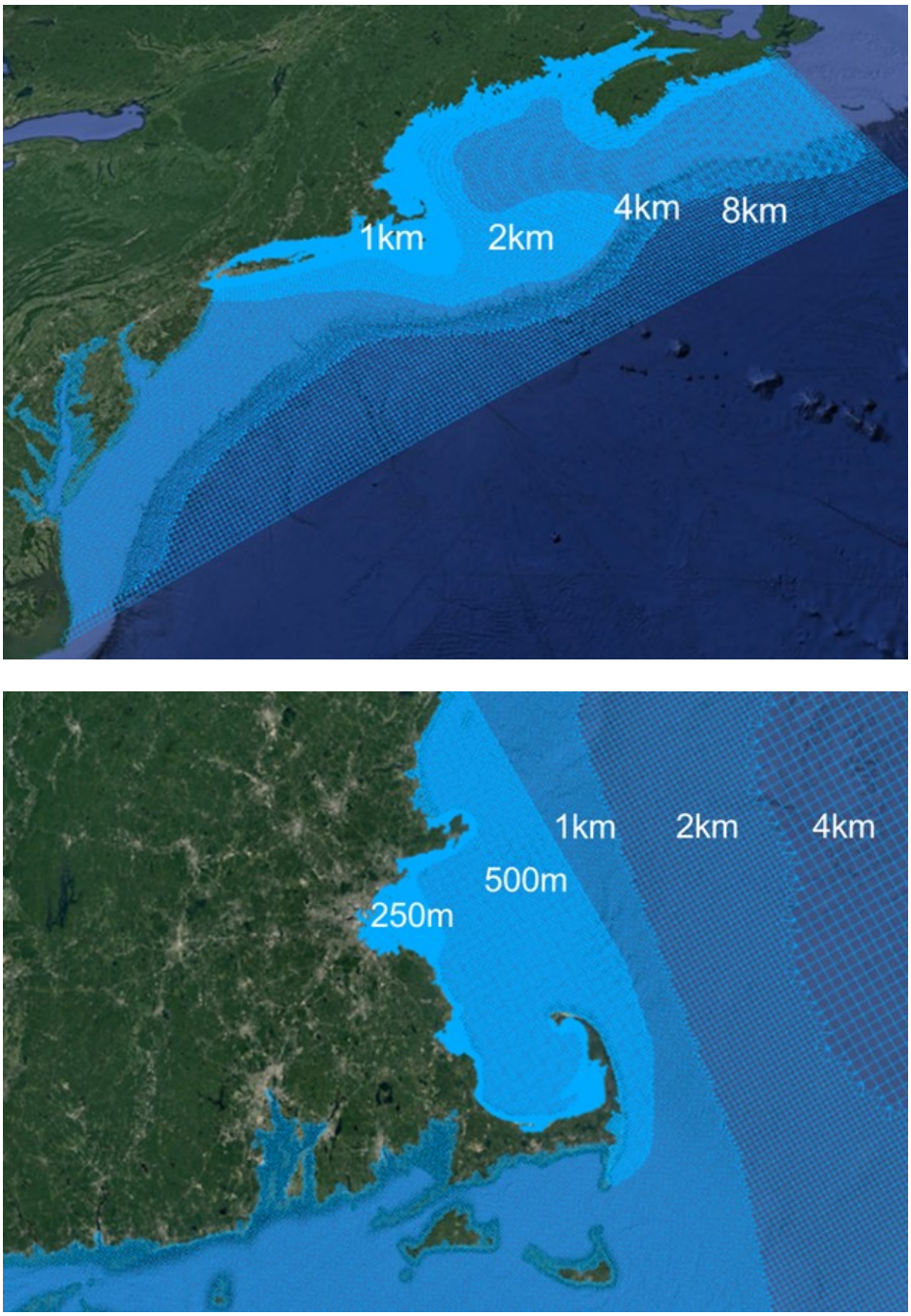

Figure A.2-1 Horizontal grid resolution in the entire updated BEM model grid (top); Zoom into Massachusetts Bay (bottom). The horizontal grid resolution ranges from 8 km offshore to 250 m in Boston Harbor and along the coast of Massachusetts Bay and Cape Cod Bay. The highest resolution areas (250m and 500m) are only visible in the bottom figure due to the density of the grid lines.

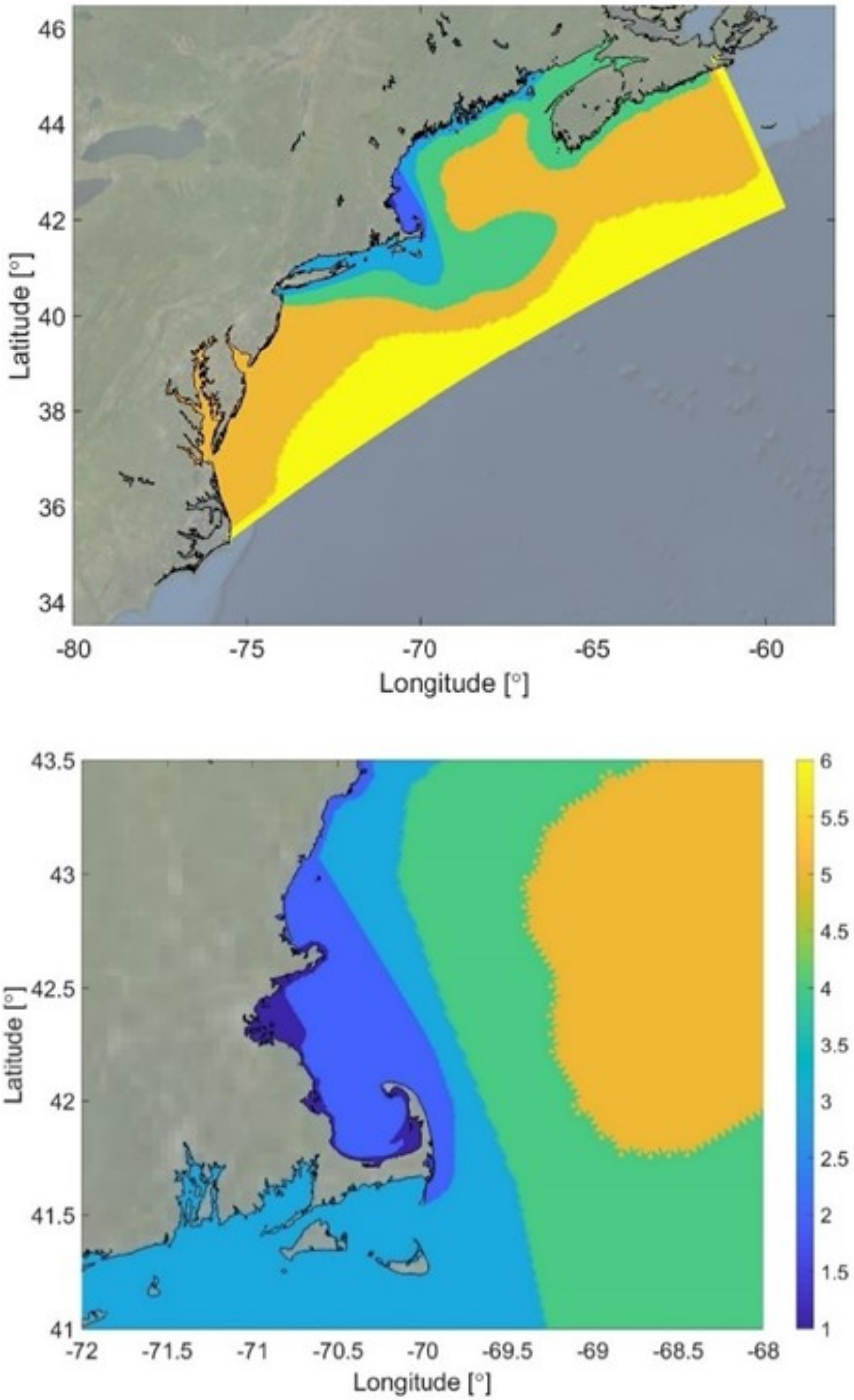

Figure A.2-2 Extent of horizontal grid resolution regions, color coded and numbered from 1 to 6 for entire model domain (top) and coastal Massachusetts (bottom). Corresponding resolutions are: yellow=6(8km); orange=5(4km); green=4(2km); light blue=3(1km); royal blue=2(500m); dark blue=1(250m)

A.2.2 Bathymetry

For the Gulf of Maine, the bathymetry used is the 3-Arcsecond Digital Elevation Model (DEM) (https://pubs.usgs.gov/of/2011/1127/), a 90m resolution gridded topography covering the majority of the model domain. The dataset is referenced to North American Vertical Datum of 1988 (NAVD88) (vertical) and North American Datum (NAD83) (horizontal) coordinates, so it has been converted to World Geodetic System 1984 (WGS84) horizontal coordinate system for consistency with the model grid.

The remainder of the model bathymetry is derived from the “ETOPO1” (Earth Topographic) Global Relief Model (https://www.ngdc.noaa.gov/mgg/global/) distributed by the National Oceanic and Atmospheric Administration (NOAA). ETOPO1 uses the NOAA Coastal Relief Model for this domain, which is the main background dataset within the above-mentioned Gulf of Maine DEM, so a high level of consistency is expected for the US territory. The model bathymetry is shown in Figure A.2-3.

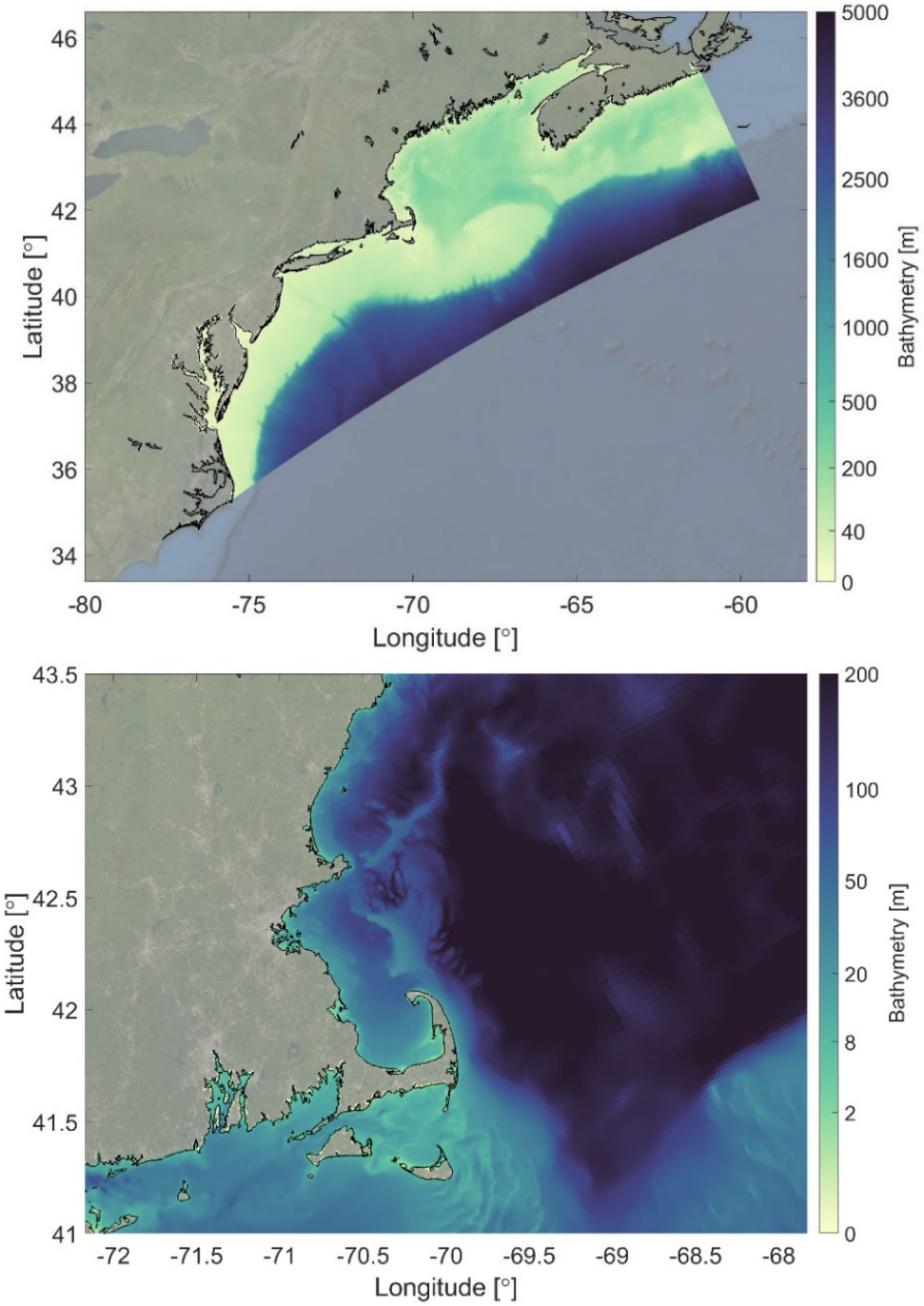

Figure A.2-3 Model bathymetry (m), consisting of the Gulf of Maine DEM and ETOPO1 datasets. Whole domain (top) and zoom into Massachusetts Bay (bottom).

A.2.3 Coastline

The land is masked through the World Vector Shoreline dataset provided by NOAA, with approximately 100m resolution for the Massachusetts coastline (https://shoreline.noaa.gov/data/datasheets/wvs.html). This land boundary file is used to conservatively remove land cells, as it will only delete cells that are entirely within the land boundary, i.e. fully in land. Those cells are literally cut-out from the grid, as shown in Figure A.2-4 (left). As only cells completely on land (positive bed level on all their corners/nodes) are cut-out through this procedure, the cells that are partially wet – meaning they cover the transition from a positive bed level (land) to a negative bed level (sea) – are the last coastal grid cell. Their cell center depth value will result from the linear interpolation between the values at the cell nodes. As wetting and drying is allowed in Delft-3D FM, these coastal cells might dry at low tide, if in intertidal areas.

A 'dry cells' file has been added around Massachusetts Bay to mask out additional coastal cells whose cell center fall on the land side of this land boundary but is missed by the conservative cutting procedure. The masking entails that, while the cell is present in the grid, computationally they become inactive. This serves to remove features captured by the high coastal grid resolution in the Bay such as coastal barrier islands, and therefore obtain a refined representation of the coastline, see Figure A.2-4 (right).

For the dry cells file, only the coastline in the mainland has been considered, and not islands. All coastal model items such as river source locations and observation locations have been adjusted, as necessary, to be consistent with the definition of the coastline.

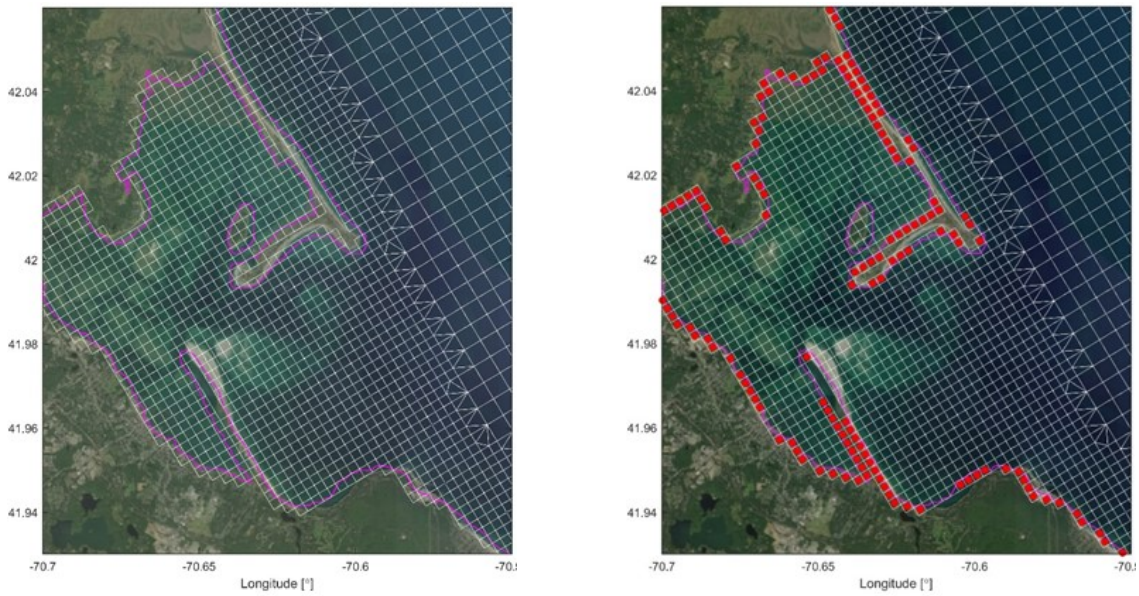

Figure A.2-4 Left: Satellite image of Plymouth MA, with model grid (white) and land boundary used to remove the land (magenta). Right: The included dry points (red dots), masking out parts of the grid that are in land but are missed by the cutting procedure.

A.3 Water Quality Configuration

A.3.1 General

The water quality component uses the advection-diffusion equation (ADE) to represent mass balances of a collection of state variables (or “substances”) in the model domain. This equation is documented in text books (Thomann and Mueller, 1987; Chapra 1996). Examples of state variables are dissolved oxygen, ammonium, particulate organic carbon, etc. In a simplified form, the ADE reads:

Change of mass = Transport by water masses + Loads ± Processes

The coefficients to describe the transport of water masses are derived from the supporting hydrodynamic component, which solves the water balance equation and the momentum balance equations in three directions (Appendix A1). The horizontal momentum balances include so-called baroclinic pressure gradients, which arise from horizontal density differences, where the density is calculated from the simulated local temperature and salinity through the equation of state.

The loads represent the inputs of state variables into the model domain, for example by rivers, by the Deer Island discharge or by atmospheric deposition.

Whereas the mathematical representation of transport and loads terms is the same for all state variables, the processes term arranges for substance-specific behavior and interactions between state variables. Processes can be of a physical or biochemical nature and can cause state variables to appear, disappear or transform from one state variable into another.

The ADE is discretized on the grid discussed in Section A.2.1, using a fixed time step. The details of the discretization method are discussed in the relevant software documentation (Deltares, 2019a,b). A key feature of the numerical approach used is strict conservation of mass. For verification, the software provides a full account of the simulated mass balance of all state variables.

The water quality modeling software used has had numerous applications world-wide since the early 1980s. Most of them are published in grey literature (e.g. van Gils et al., 2007). Some more recent journal publications are provided by Los et al. (2008), Blauw et al. (2009) and Smits and van Beek (2013).

A.3.2 Selected configuration

This section discusses the selection of state variables and processes for the water quality component.

The main features of the water quality component are derived from the Generic Ecological Model for estuaries and coastal waters by Blauw et al. (2009). The substances and processes included in the model are schematically shown in Figure A.3-1. The substances are listed in Table A.3-1. In the model configuration, the substances related to particulate organic matter represent both organic matter from

coastal discharges and detritus formed after phytoplankton mortality. All sediment associated substances are not subject to transport (i.e. they are fixed on the grid) and they are restricted to the bottom grid layer.

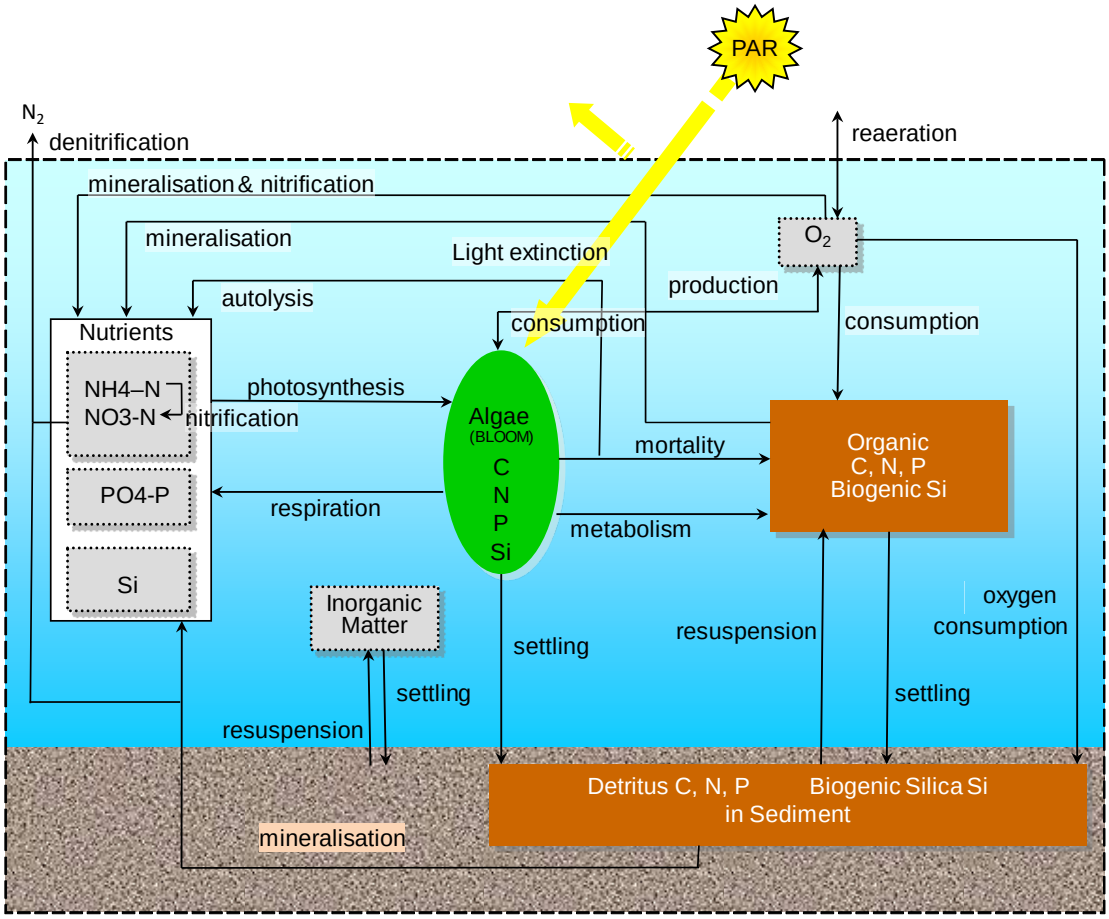

Figure A.3-1 Schematic overview of all state variables and processes (modified from Blauw et al,. 2009). Note that light extinction in the water column is affected by Particulate Inorganic Matter, Algae, and Detritus (brown box in water column labeled "Organic C, N, P Biogenic Si").

The physical and biogeochemical processes shown in Figure A.3-1 comprise:

- The photosynthesis by phytoplankton, and the associated uptake of nutrients and production of oxygen, supported by photosynthetically active radiation (PAR) penetrating into the water column;
- Phytoplankton respiration, metabolism and mortality, and the associated release of nutrients (partly detritus, partly inorganic) and consumption of oxygen;
- The mineralization of organic matter (detritus) in the water column and in the sediment, both leading to consumption of oxygen;
- The dissolution of Biogenic Silica in the water column and in the sediment;
- The settling of organic matter, inorganic particles and phytoplankton;

- The resuspension of sediment by currents or wave action;
- Exchange of oxygen into and out of the air-sea interface (reaeration);
- Nitrification and the associated consumption of oxygen;
- Denitrification, in the water column and in the sediment.

Table A.3-1 List of state variables in the water quality component.

State variable	Name in the model
Dissolved oxygen (DO)	OXY
Particulate organic matter (C, N, P), biogenic silica (Si)	POC1, PON1, POP1, Opal
Dissolved organic matter (C, N, P)	DOC, DON, DOP
Particulate inorganic matter	IM1
Dissolved inorganic matter	NH4, NO3, PO4, Si
Four functional groups of pelagic phytoplankton (diatoms, dinoflagellates, other flagellates, phaeocystis), each represented by 3 phenotypes (X = E, N, P; see section A3.3.1 for more details)	MDIATOMS_X, DINOFLAG_X, MFLAGELA_X, PHAEOCYS_X
Particulate organic matter (C, N, P) and biogenic silica (Si) in sediment	POC1S1, PON1S1, POP1S1, OpalS1

The physical and biogeochemical processes formulations are provided in Appendix A2 (modified from Blauw et al., 2009). The water quality model uses process representations selected from the Delft3D-FM Water Quality Process Library. A full account is available in the Delft3D-WAQ documentation (Deltares, 2014).

A.3.3 Current approach relative to the former BEM

The selected configuration deviates somewhat from the former BEM as described in Zhao et al., 2017 and the references therein. In some cases, the formulations have been expanded, whereas in other cases they have been simplified. An overview is provided below of some key aspects of the selected configuration and a discussion of the motivation behind these choices is provided.

A.3.3.1 Phytoplankton model

The phytoplankton sub-model, named “BLOOM” (Los, 2009), simulates primary production, respiration and mortality of phytoplankton. Within each functional group represented in the model (Table A.3-1), three phenotypes are defined to account for adaptation to changing environmental conditions:

1. An energy type ("_E"), with relatively high growth rate, low mortality rate and high N/C and P/C ratio, and higher chlorophyll content;
2. A nitrogen type ("_N"), with typically lower internal N/C ratio, lower maximum growth rate, higher mortality rate, higher settling velocity and lower chlorophyll-a content;
3. A phosphorus type ("_P"), similar to the nitrogen type with typically lower internal P/C ratio.

BLOOM assumes that fast-growing phytoplankton (energy type) dominate in situations where light and nutrient resources are abundant, while slow-growing, efficient phytoplankton species become dominant when resources become limited (Blauw et al., 2009). When conditions in the water change, one phenotype can be instantaneously converted into another phenotype of the same functional group. This represents the rapid adaptation of individual algal cells. Species composition is calculated using linear programming to maximize the total net production of the whole phytoplankton community, depending on the prevailing conditions. Further details can be obtained from Los (2009). Parameters and equations are provided in Appendix A2.

The BLOOM model was selected because it (a) allows for flexibility with respect to the number and nature of algae groups; and (b) features variable nutrient to carbon, and chlorophyll to carbon ratios. Parameterizations are available for many commonly encountered groups as a starting point for the updated BEM. BLOOM has a long track record in North Sea eutrophication models, see for example the related summary in Chapter 8 of Los (2009).

A.3.3.2 Attenuation of light

The vertical attenuation of PAR in the water column is represented by a linear extinction model. The former BEM used the same concept. In the former BEM, the extinction coefficient (the fraction of light disappearing per unit of vertical path length), was represented by a spatially variable background contribution and a "self-shading" contribution by living phytoplankton. The background contribution was supposed to represent contributions by inorganic and organic suspended and dissolved substances (other than phytoplankton). This leads to a relatively stable simulated extinction coefficient while field data showed more variability (Figure A.3-2).

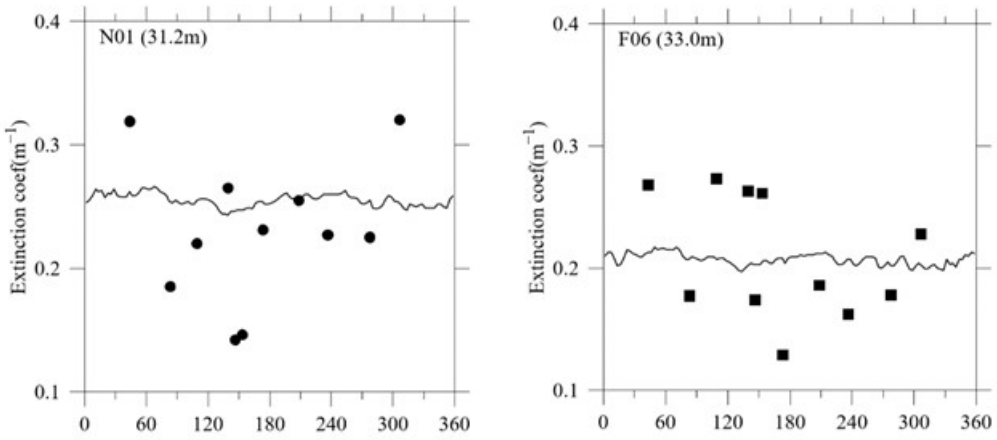

Figure A.3-2 Simulated vs observed extinction coefficient for the year 2016 (day number on x-axis) at selected stations (N01-left and F06-right; for station map see Figure 2-1 in the main report). These are results from the former BEM 2016 simulation (copied from Zhao et al., 2017).

As the varying (in space and time) availability of light and nutrients could well be important for phytoplankton dynamics, and as phytoplankton dynamics could well be important to assess the impacts from the Deer Island discharge, it was decided to include the temporal variability of the non-algal part of the extinction coefficient.

Initial evaluation of available measurements revealed a correlation between light extinction and total suspended solids (TSS), a very common phenomenon for relatively shallow coastal areas (see Figure A.3-3 using observations from Boston Harbor). Therefore, the background extinction is made dependent on the ambient concentrations of organic and inorganic particles. To this end, a state variable was added to represent inorganic particles in the water column, and a spatially variable pool of bottom fine sediment particles is included. These particles resuspend into the water column when and where conditions are suitable and slowly re-settle afterwards, temporally contributing to light extinction. See Section A.3.4 for more details on resuspension modeling.

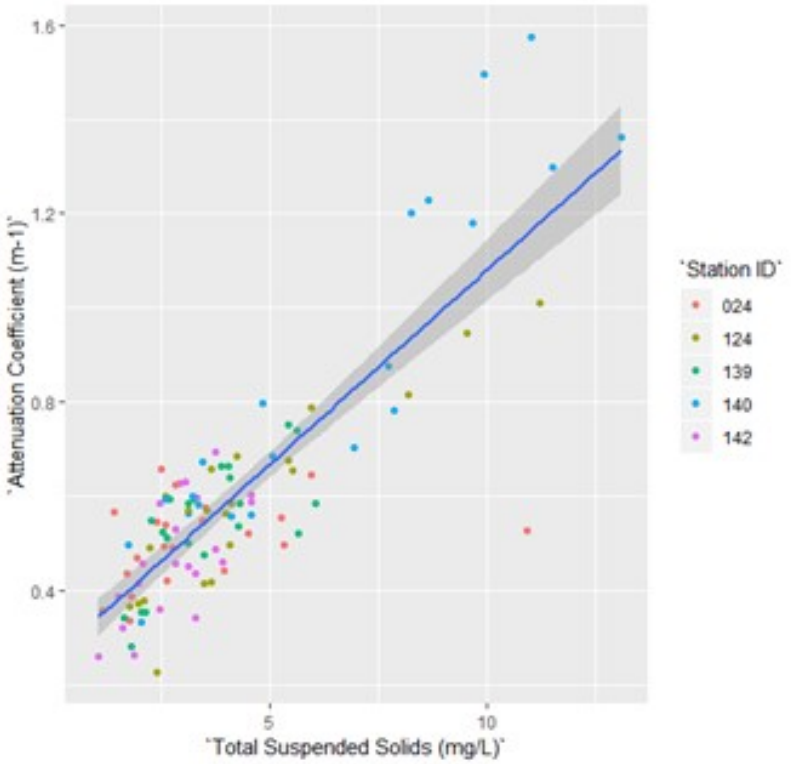

Figure A.3-3 Regression between observed values of TSS and Extinction Coefficient for Boston Harbor stations in 2016 (for station map, see Figure 2-1 of the main report). The blue line is the best-fit linear model and the shading its 95% confidence interval.

A.3.3.3 Representation of organic matter

A single fraction of particulate organic matter represents both the particulate organic matter from the discharge and detritus. This is considered feasible since the effluent has undergone treatment and shows relatively low concentrations of organic matter. The very rapidly settling and decaying fractions of organic waste are expected to be already removed by the treatment process and do not require an extra fraction of organic matter in the model. Moreover, the use of multiple fractions of particulate organic matter with their own settling and decay rates is difficult to validate on observations of particulate organic carbon (POC) or biological oxygen demand (BOD) alone and easily leads to an over-parameterized model.

To avoid over-parameterization, just a single dissolved organic nitrogen (DON) pool was added. This pool represents the more stable organic N next to the more labile PON formed after mortality of phytoplankton (as also used by Adams et al., 1992). To maintain consistency, dissolved organic carbon (DOC) and dissolved organic phosphorous (DOP) pools were added as well. Figure A.3-4 provides a summary of the currently used configuration.

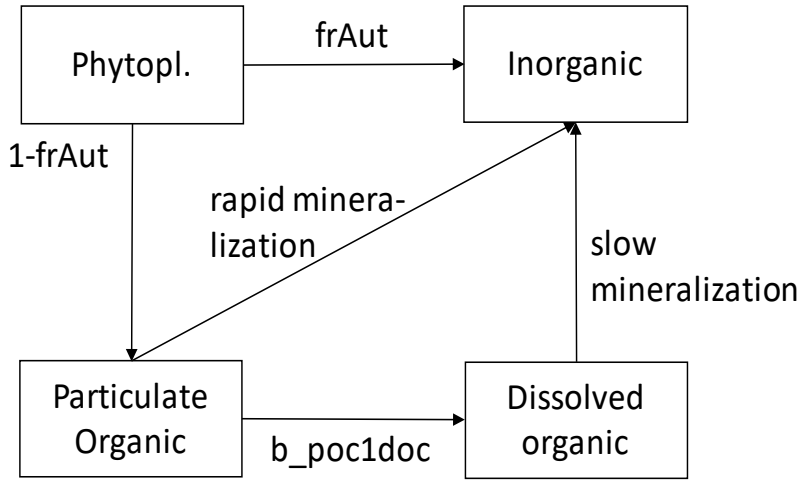

Figure A.3-4 Schematic representation of the nutrients recycling model components in the selected Delft3D-FM configuration. frAut ("fraction autotrophic") is the fraction of dying phytoplankton that is directly re-mineralized; b_poc1doc represents the conversion of particulate organic matter (POM) to dissolved organic matter (DOM), expressed as a fraction of the rapid mineralization flux.

Phytoplankton mortality is distributed over the particulate organic and inorganic pools (frAut=0 for C and frAut=0.3 for N and P). Mineralization of particulate organic matter (POM) is calibrated (empirically determined using comparisons of model output to field measurements). The flux to dissolved organic matter (DOM) is equal to the POM mineralization flux, multiplied with b_poc1doc. The mineralization of DOM is calibrated.

A.3.3.4 Sediment diagenesis

For the representation of sediment diagenesis (release of nutrients as a result of settling of organic matter), there appears to be no reason to deviate from the standard Delft3D approach (referred to as S1/2, see Deltares, 2020) as is used routinely in North Sea applications.

In this approach, bottom sediment is not included as a separate layer in the model grid. Only relevant settled particulates (POC1S1, PON1S1, POP1S1 and OpalS1; Table A.3-1) are simulated as additional model state variables. Porewater concentrations of dissolved constituents are not calculated; remineralized nutrients are therefore directly released back to the water column, and the oxygen consumed for the mineralization of benthic organic matter is directly drawn from the water column. Settled organic matter can also be buried to deeper sediment, and not be available for transformation in the model any more.

A.3.4 Resuspension modeling

Where and when the shear stress (τ; N m^{-2}) is high enough, the top sediment layer is resuspended. Following resuspension, the coarse particles re-settle quickly, while the fine particles remain in suspension for some time and thus affect the attenuation of light. The critical shear stress for resuspension expresses the susceptibility of the sediments

to be resuspended from the seabed into the water column. The equations describing resuspension processes and resuspension flux are given in Appendix A2.2.

The shear stress is the cumulative result of currents and waves, which is used for the resuspension of particles from the top sediment layer. The bed shear stress induced by currents is equal to the bottom friction experienced by the currents in the hydrodynamic part of the model. In order to include wave induced resuspension without running extensive wave simulation models, waves are assumed to be locally generated wind waves in deep water. Wave heights are then computed based on the wind speed, the water depth and the fetch. Here, the fetch is dependent on the wind direction (i.e. discretized to 12 bins of 30°) and determined by the model for each grid cell as the distance to the first dry point when looking into the direction where the wind is coming from. Wave height and period are then computed according to formulations by Hurdle & Stive (1989). The wave induced bed shear stress is computed from the orbital velocity.

This approach provides the resuspension flux of total sediment (dry matter) for all sediment components. The resuspension flux for each individual component is proportional to this total resuspension, based on its fraction in sediment dry matter. The fraction of inorganic fines (IM1) in the sediment is not simulated: it is forced using a 2D map of the seabed sediment composition (see Section A.8.1).

A.3.5 Numerical aspects

The water quality component needs to deal with different physical and biochemical processes, which are simulated using different time steps. The transport of substances is simulated in exactly the same way as the transport of salt and heat. The time step is variable, depending on local and current conditions. To allow the model to produce output at fixed user-defined time intervals, a time step called “DtUser” is defined. In the updated BEM, DtUser equals 10 minutes.

The biochemical processes discussed in this section are computed using a time step called “DtProcesses”. DtProcesses needs to be a whole multiple of DtUser. In the updated BEM, DtProcesses equals DtUser.

The phytoplankton sub-model deviates from the above as phytoplankton dynamics are parameterized based on a daily average basis. Therefore, this sub-model runs with a time step equal to a whole multiple of DtProcesses. In the updated BEM, this multiplier equals 144, as 144 times 10 minutes equals 24 hours.

Numerically, these three clusters of processes are integrated using the so-called “fractional step method”. In the updated BEM, this proceeds as follows. Smaller transport timesteps are made until the next multiple of DTUser is reached. At that moment, a separate biochemical processes timestep is made (since DtProcesses = DtUser). Every 144th DtProcesses step, the phytoplankton sub-model conducts its larger time step. The advantage of this method is that it is unconditionally stable if the separate fractional steps are stable. This method has proven its merits in numerous practical applications of Delft3D (with both regular grid and flexible mesh versions) carried out since the late 1990s.

A.4 Outfall

A.4.1 Water discharge

The outfall is introduced in the model using the horizontal locations and depths of the 55 risers as provided by MWRA (see Appendix A3). The location of the effluent diffuser array in the model grid is shown in Figure A.4-1.The total discharge provided by MWRA is evenly divided over the 55 risers, and the temperature is also included as specified in the provided data. As the model resolution in the area of the diffuser is approximately 250 meters, there are multiple risers in one grid cell. Delft3D FM automatically snaps the 55 source points to the closest cell centers during the simulation initialization. When multiple discharges are associated to the same cell center, these are added together.

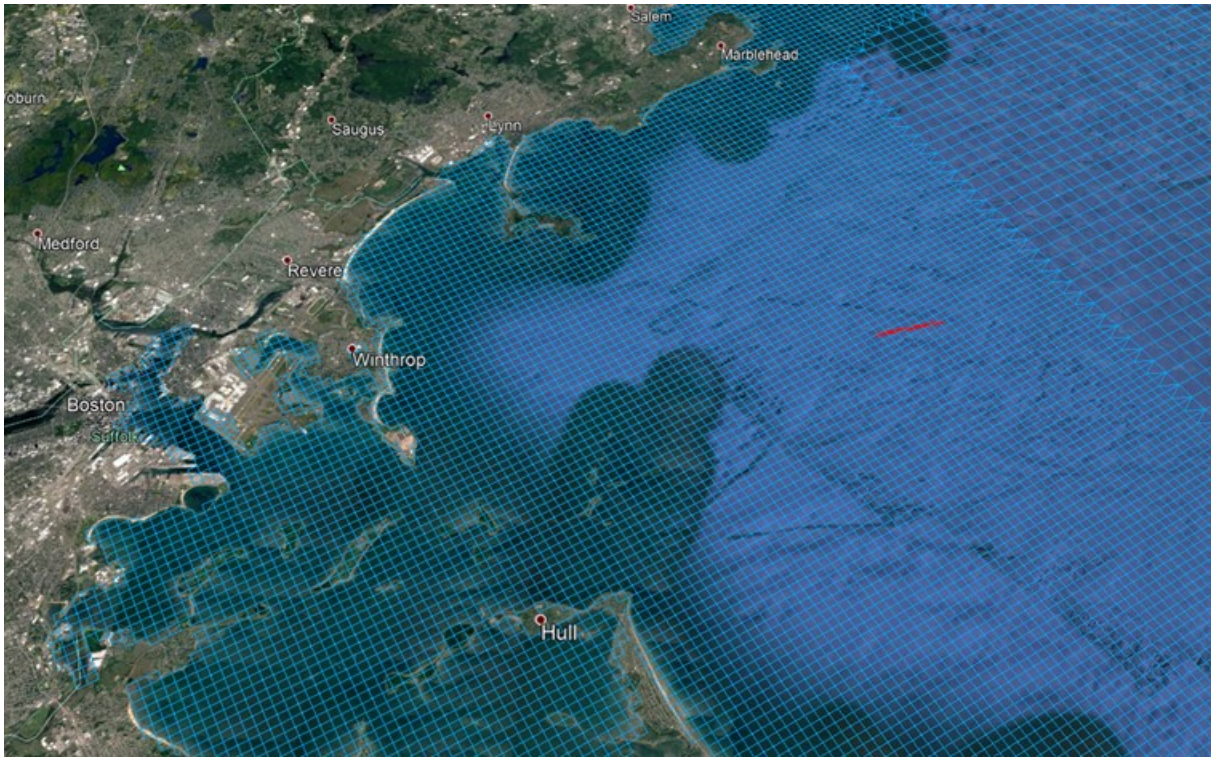

Figure A.4-1 Effluent diffuser array (red) and model grid (blue) in Boston area. The total MWRA-outfall discharge is evenly distributed over the 55 risers. The model grid has a resolution of 250m in the area of the outfall. The exact location of the risers and their bathymetric depths are given in Appendix A3.

A.4.2 Loads

MWRA measures the daily concentrations of carbonaceous Biochemical Oxygen Demand (CBOD), total Kjeldahl nitrogen (TKN), ammonia (NH_3), nitrites (NO_2), nitrates (NO_3), orthophosphates (PO_4) and total phosphorus (TP) in the effluent. These are used to define the concentrations of all modeled substances, see Table A.4-1.

Table A.4-1 Conversion factors from measured parameters to BEM modeled substances for the definition of the MWRA outfall load.

State variable	Descriptive Name	Effluent concentration in MWRA outfall
OXY	Dissolved Oxygen (DO)	80% of saturation (**note 1**)
POC1	Particulate Organic Carbon	measured CBOD * 0.6 / 2.67 (**notes 2, 3**)
DOC	Dissolved Organic Carbon	measured CBOD * 0.4 / 2.67 (**notes 2, 3**)
PON1	Particulate Organic Nitrogen	MAX((measured TKN – measured NH_3) × 0.6, 0.) (**note 3**)
DON	Dissolved Organic Nitrogen	MAX((measured TKN – measured NH_3) × 0.4, 0.) (**note 3**)
NH4	Ammonium	measured NH_3
NO3	Nitrate	measured NO_2 + measured NO_3
POP1	Particulate Organic Phosphorus	MAX((measured TP – measured PO_4) × 0.8, 0.) (**note 4**)
DOP	Dissolved Organic Phosphorus	MAX((measured TP – measured PO_4) × 0.2, 0.) (**note 4**)
PO4	Phosphate	measured PO_4
Si	Dissolved inorganic silica	4.10 mgSi/L (**note 5**)
Opal	Biogenic silica	0.0
IM1	Inorganic suspended Matter	0.0
Phyto-plankton	phytoplankton	0.0

1 Using the same equation for oxygen saturation as a function of salinity and temperature as in the water quality component, salinity=0.1 and measured temperature (see Eq. A2.46 in Appendix A2). Oxygen is not measured, but the effluent is likely well aerated even after travel through the outfall tunnel, given the nature of the treatment process and the discharge configuration.

2 2.67 is the ratio between O_2 and C in the oxidation reaction.

3 The proportion of DON:PON is determined based on measurements at MWRA monitoring station N21. TDN, NH4, (NO3+NO2) and PON measurements are available. At each sampling date, DON=MAX(TDN-NH4-(NO3+NO2), 0.). Assuming that the relationships between DON and salinity and PON and salinity represent the footprint of the fresh DITP discharge, it follows that there is about 1.5 times as much PON as there is DON in DITP (Figure A.4-2). Therefore a DON:PON ratio of 0.4:0.6 is used. The same ratio is applied for DOC:POC.

4 Similarly, the DOP:POP ratio is estimated based on measurements of TDP, PO_4 and particulate phosphorus (PP) at station N21. DOP and POP are calculated as: DOP=MAX(TDP-PO_4, 0.) and POP=PP. Assuming that changes along the salinity gradient represents the signature of the DITP outfall, DOP:POP in the DITP is ~0.2:0.8 (Figure A.4-2).

5 2014 Annual mean (Maguire and Fulweiler, 2017).

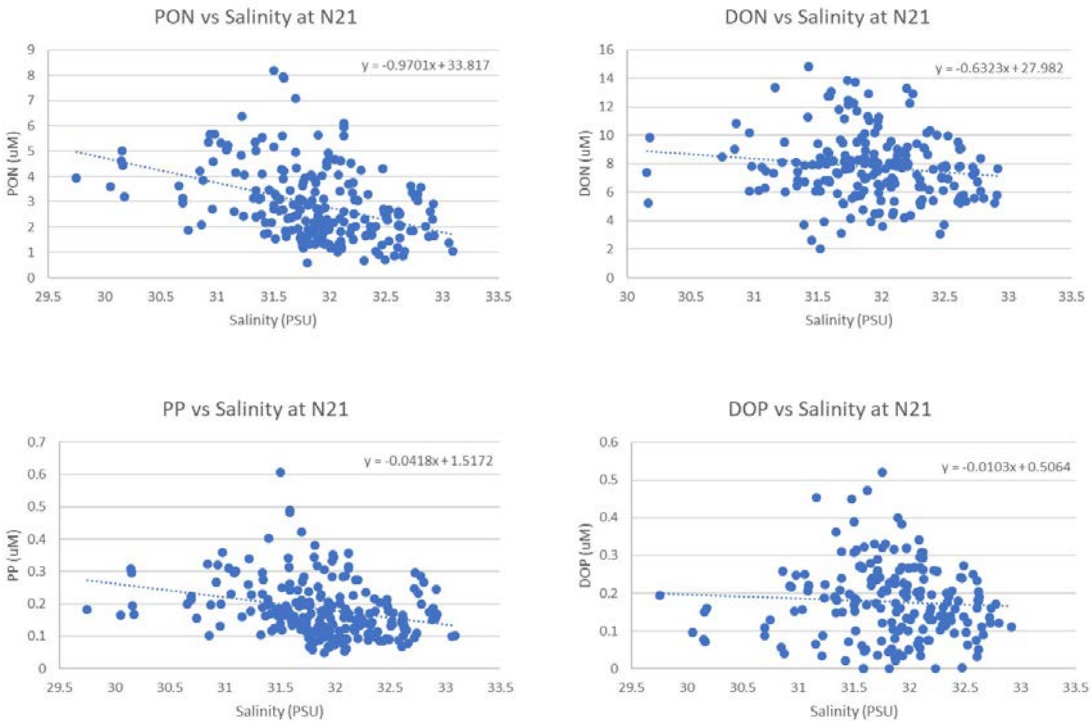

Figure A.4-2 Relation between the dissolved and particulate organic pools of nitrogen, and particulate phosphorus and dissolved organic phosphorus derived from analysis results from MWRA station N21 (close to the outfall) and salinity.

A.5 River inputs

A.5.1 Rivers included

The river discharges for 19 major rivers are included in the model. These rivers are all to the north of Massachusetts Bay, while rivers to the south of Mass Bay are not included in the model. Because of the prevailing residual flow direction, the latter are expected to have a negligible influence on the conditions in this area of interest. Measured flows have been downloaded from the US Geological Survey (USGS) database (https://waterdata.usgs.gov/nwis) and formatted for input into the model. Table A.5-1 shows the station names and identification numbers, average discharges for the period 2011-2018 as well as the number of missing datapoints based on the average time-step detected (15 minutes for all stations) and largest gaps in days.

Table A.5-1 Overview of river stations and their discharge as included in the model, also identifying major data gaps in available data. Source: USGS database (https://waterdata.usgs.gov/nwis). These discharge values are for the location of the gauge, before adjustment.

Station	mean discharge [m3/s]	ave. tstep [min]	no. missing	max. gap [days]
st.john_01014000	359.36	15	105498	154
st.croix_01021000	84.50	15	31252	49
penobscot_01034500	405.37	15	83551	135
androscoggin_01059000	188.68	15	14730	61
kennebec_01049265	295.83	15	69135	133
saco_01066000	85.19	15	52389	106
isinglass_01072870	3.46	15	46207	86
winnicut_01073785	0.67	15	44149	169
lamprey_01073500	8.04	15	18209	44
exeter_01073587	2.64	15	33079	54
merrimack_01100000	238.19	15	11988	15
parker_01101000	0.98	15	20728	67
ipswich_01102000	4.84	15	5441	14
saugus_01102345	0.79	15	12302	19
mystic_01103010	NA *	NA	NA*	NA
charles_01104500	8.81	15	755	3
neponset_011055566	8.46	15	114381	72
north_01169000	6.64	15	38943	85
jones_01105870	0.87	15	19758	7

* No measurements for the period 2011-2018; Discharge is estimated as a fraction of the Charles discharge, based on ratios of flow in Alber and Chan (1994), see text for full explanation.

A.5.2 Gaps in discharge measurements

Measurements downloaded from the USGS site for the period of 2011-2018 showed a considerable number of data gaps, as presented in the table above. An analysis of the distribution of the data gaps shows significant spread, ranging from 3 days (Charles River) to 169 days (Winnicut River).

For small data gaps of less than 3 days, the gaps are filled through linear interpolation. Larger gaps are treated by regression against neighboring rivers and using the river with the best R^2 correlation value. This is done iteratively until all gaps are filled. Most data gaps could be filled with this approach; however, it is to be mentioned that correlation was often quite low between the rivers for the selected period and available data (Figure A.5-1).

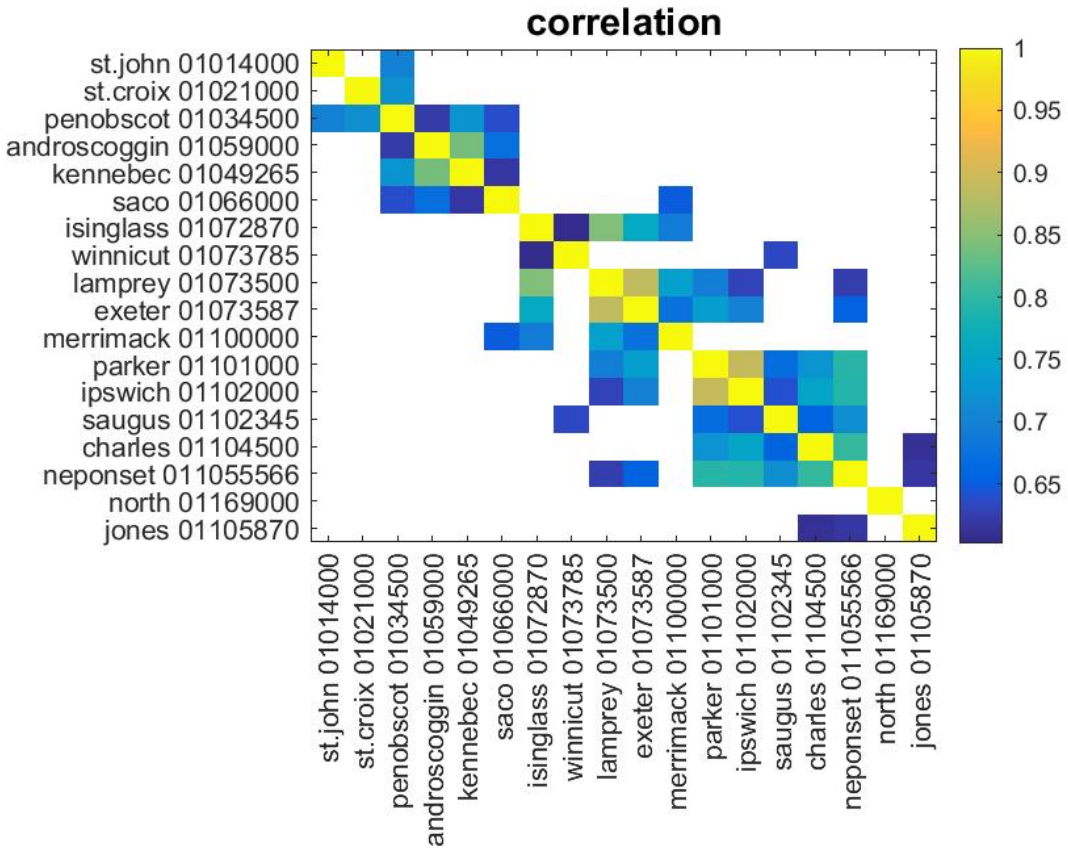

Figure A.5-1 R2 (symmetric) matrix when cross-correlating all rivers in the model, from north to south. Values lower than 0.6 are removed for visualization. Note that Mystic River is omitted due to lack of measurements there (see text for explanation).

Lastly, the time-series are evaluated again for gaps smaller than 3 days and filled through linear interpolation.

For the Mystic River, no measurements were available from the USGS for the time period of interest. The Mystic River discharge is set to 0.195 times the gap-filled, adjusted (see next section) Charles River discharge, based on the ratio of the flows in Alber and Chan, 1994).

A.5.3 Adjusted river discharges

In addition to filling the data gaps, some other modifications have been made to the original USGS river flow values such as scaling of discharge and combining rivers.

Scaling factors

For a number of rivers, a scaling factor has been applied to the measured discharge to compensate for the upstream location of the gauging station relative to the coast, thus accounting for the watershed area downstream of the gauge. Table A.5-2 gives an overview of the applied scaling factors, all of which were provided by MWRA and based on Table 2-1 of Signell, Jenter, and Blumberg USGS Report 96-015

(https://pdfs.semanticscholar.org/f50b/8aba2ccb144912e2696377ddc53536294870.pdf). For the Charles River, a scaling factor of 1.13 is used, based on Hydroqual and Normandeau (1995) and Alber and Chan (1994).

Table A.5-2 Overview of scaling factors used for a number of river stations, from north to south. The scaling factors are applied to compensate for the upstream location of the gauging station relative to the coast.

River ID	Scale factor
penobscot_01034500	1.10
androscoggin 01059000	1.15
kennebec_01042500	1.15
saco_01064500	1.31
merrimack_01100000	1.08
charles_01104500	1.13

Combining river discharges
The discharges from some of the smaller rivers have been combined where the model grid did not have sufficient resolution to include them separately (see Table A.5-3). In particular:

- exeter_01073587, winnicut_01073785, lamprey_01073500 and isinglass_01072870 were added together and also scaled by a factor of 2.92 to estimate the Piscataqua River discharge (this is called 'Piscataqua' in the river inputs),
- kennebec_01042500 and androscoggin_01059000 were added together, and called 'Kennebec' in the river inputs,
- ipswich_01102000 and parker_01101000 were added together and called 'Ipswich' in the river inputs.

Flow from the Piscataqua River is estimated by applying the scale-up factor 2.92, to account for ungauged areas, to the sum of the flows from the USGS gauges for the Isinglass (#01072870), Lamprey (#01073500), Exeter (#01073587), and Winnicut (#01073785) rivers. These rivers include drainage from a fraction of the total watershed for the Piscataqua River. The Isinglass, Lamprey, and Winnicut gauges are located near the downstream limits of their respective watershed areas (75, 215, and 17.5 square miles; NH DES, 2019a,b; ESRLAC, 2012) and assumed to include runoff from their entire watershed. The Exeter gauge is located roughly in the middle of the Exeter-Squamscott watershed (128 square miles; NH DES 2019) and is assumed to include runoff from half of its area. The scale-up factor 2.92 is the ratio of the total area of the Piscataqua River watershed (1086 square miles; PREP 2012) to the summed area attributed to the four gauges (371.5 square miles).

The listed scale factors were applied before combining the discharges.

The discharge locations have been relocated when needed for an appropriate forcing into the model grid. This means sources located originally upstream have been located at cells best representing the connection of the river mouth and the sea. The final coordinates are shown in Figure A.5-2 and Table A.5-3.

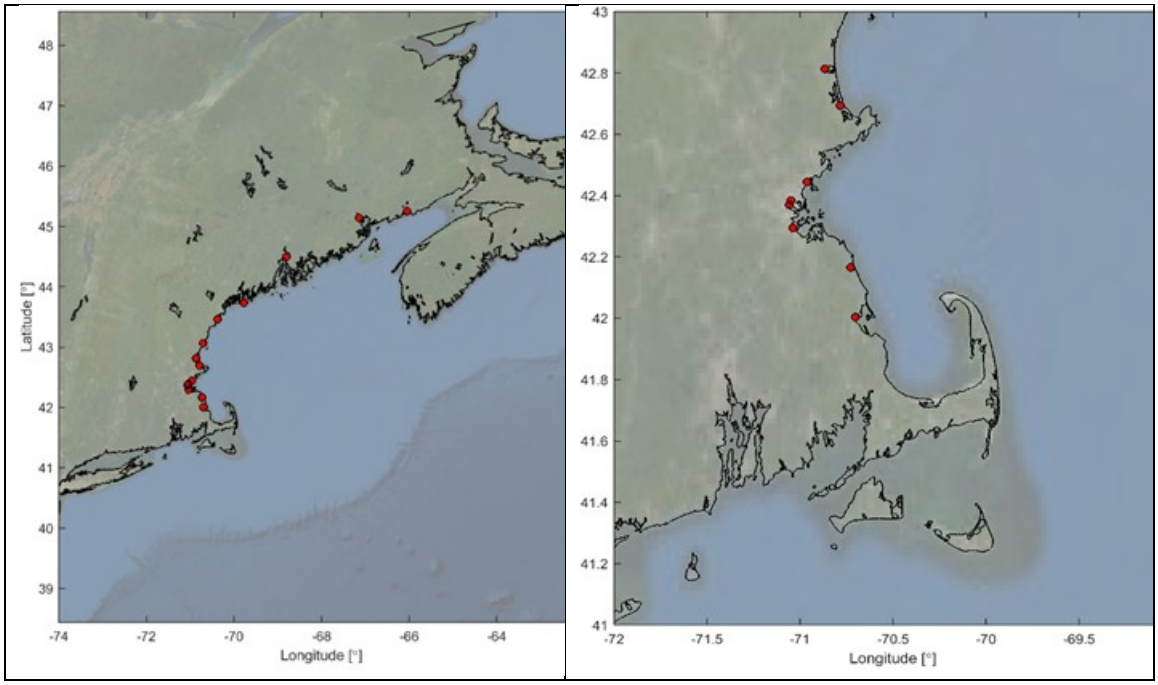

Figure A.5-2 River discharge locations (14 in total) on the Gulf of Maine (left) and zoom into Massachusetts Bay (right). Table A.4 3 lists the corresponding source names.

Table A.5-3 River discharge locations (coordinates) in the updated BEM, from north to south.

River ID	longitude	latitude
st.john_01014000	-66.0416	45.2506
st.croix_01021000	-67.1426	45.1396
penobscot_01034500	-68.7989	44.4984
kennebec_01042500*	-69.7729	43.7372
saco_01064500	-70.3741	43.4655
Piscataqua**	-70.7070	43.0670
merrimack_01100000	-70.8671	42.8139
ipswich_01102000***	-70.7825	42.6936
saugus_01102345	-70.9624	42.4448
mystic_01103010	-71.0483	42.3846
charles_01104500	-71.0576	42.3704
neponset_011055566	-71.0381	42.2945
north_01169000	-70.7276	42.1660
jones_01105870	-70.7019	42.0040

*added Kennebec and Androscoggin discharges

** Piscataqua River discharge is estimated by adding Isinglass, Exeter, Winnicut and Lamprey discharges, and scaling this by a factor 2.92.

***sum of Ipswich and Parker discharges

A.5.4 River nutrient loads

A.5.4.1 Charles, Neponset and Mystic rivers

Measured concentrations of chlorophyll-*a* (Chl-a), dissolved oxygen (DO), ammonium (NH_4), oxidized nitrogen (NO_2+NO_3), phosphates (PO_4), silicates (SiO_4), total nitrogen (TN), total phosphorus (TP) and total suspended solids (TSS) are available for 2012-2016 for the Charles, Neponset and Mystic rivers at a 2-week time step (provided by MWRA). For these rivers, the conversion from measured parameters to BEM modeled substances is defined in Table A.5-4.

Table A.5-4 Conversion factors from measured parameters to BEM modeled substances for the definition of the Charles, Neponset and Mystic river loads.

State variable	Descriptive Name	River concentration
OXY	Dissolved Oxygen	measured DO
POC1	Particulate Organic Carbon	PON1 × 12 (**note 1**)
DOC	Dissolved Organic Carbon	DON × 12 (**note 1**)
PON1	Particulate Organic Nitrogen	MAX(measured TN – measured NH_4 – measured NO_2+NO_3, 0.) × 0.31 (**note 2**)
DON	Dissolved Organic Nitrogen	MAX(measured TN – measured NH_4 – measured NO_2+NO_3, 0.) × 0.69 (**note 2**)
NH4	Ammonium	measured NH_4
NO3	Nitrate	measured NO_2 + NO_3
POP1	Particulate Organic Phosphorus	MIN(PON1 * 12/46 (note 1); MAX(measured TP – measured PO_4, 0.)) × 0.64 (**note 3**)
DOP	Dissolved Organic Phosphorus	MIN(PON1 * 12/46 (note 1); MAX(measured TP – measured PO_4, 0.)) × 0.36 (**note 3**)
PO4	Phosphate	measured PO_4
Si	Dissolved inorganic silica	measured SiO_4
Opal	Biogenic silica	0.0
IM1	Inorganic suspended Matter	MAX(measured TSS – POC1 × 2.5 , 0.) (**note 4**)
Phyto-plankton	phytoplankton	0.0

1 POC concentrations are calculated using weight C:N ratio of 12 mgC/mgN, as reported by Meybeck (1982) for TOC in world rivers.

2 The proportion of DON:TON is determined based on measurements at the harbor monitoring stations 124, 139 and 140, at dates where TDN, NH_4, (NO_3+NO_2) and PON measurements are available. At each sampling date, DON=MAX(TDN-NH_4-(NO_3+NO_2), 0.) and TON=DON+PON (Figure A.5-3). The average DON:TON ratio for 2012-2016 is 0.69. The same ratio is applied for DOC:TOC.

3 Similarly, at each sampling date where TDP, PO_4 and particulate phosphorus (PP) are measured, DOP and TOP are calculated as: DOP=MAX(TDP-PO_4, 0.) and TOP=DOP+PP (Figure A.5-3). The average DOP:TOP ratio for 2012-2016 is 0.36.

4 The conversion factor from C to dry mass for organic matter is assumed 2.5.

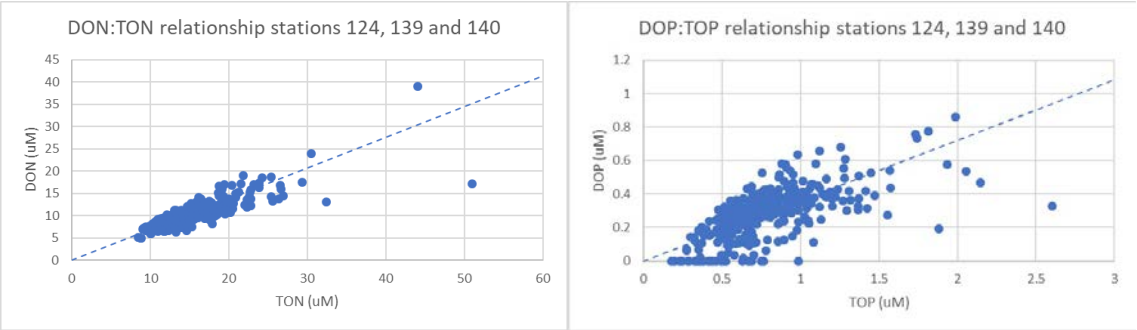

Figure A.5-3 Relation between the dissolved and total organic pools of nitrogen and phosphorus derived from analysis results from MWRA stations 124, 139 and 140 (near the mouth of the Charles, Neponset and Mystic rivers). The dotted lines correspond to DON:TON=0.69 and DOP:TOP=0.36.

A.5.4.2 Merrimack River

The same parameters were measured for 6 grab samples in the Merrimack River during 2017 (Bridges and Dombroski, 2018). From the 6 available stations, MO26 is used, being the most downstream station out of the saline intrusion zone. Table A.5-5 shows how the available measurements are used to derive concentrations of all modeled substances.

Table A.5-5 Conversion factors from measured parameters to BEM modeled substances for the Merrimack River loads.

State variable	Descriptive Name	River concentration
OXY	Oxygen	measured DO
POC1	Particulate Organic Carbon	PON1 × 12 (**note 1**)
DOC	Dissolved Organic Carbon	DON × 12 (**note 1**)
PON1	Particulate Organic Nitrogen	MAX(measured TN – measured (NH_3+ (NO_2+NO_3), 0.) × 0.31 (**note 2**)
DON	Dissolved Organic Nitrogen	MAX(measured TN – measured (NH_3 + (NO_2+NO_3)), 0.) × 0.69 (**note 2**)
NH4	Ammonium	measured NH_4
NO3	Nitrate	measured NO_2 + measured NO_3
POP1	Particulate Organic Phosphorus	MAX(MIN(PON1 × 12/46 (**note 1**); measured TP – measured PO_4), 0.) × 0.64 (**note 2**)
DOP	Dissolved Organic Phosphorus	MAX(MIN(PON1 × 12/46 (**note 1**); measured TP – measured PO_4), 0.) × 0.36 (**note 2**)
PO4	Phosphate	measured PO_4
Si	Dissolved inorganic silica	2.2 mg/L as Si (**note 3**)
Opal	Biogenic silica	0.0
IM1	Inorganic suspended matter	measured TSS – POC1 * 2.5 (**note 4**)
Phyto-plankton	Phytoplankton	0.0

1. ON and OP concentrations are calculated using weight C:N and C:P ratios of 12 and 46, as reported by Meybeck (1982) for TOC in world rivers.
2. The same DOM:TOM ratios are used as for the Boston Harbor rivers (based on measurements at harbor stations).
3. Median dissolved silica concentration measurement for the Merrimack River reported by Campo et al. (2003).
4. Conversion factor from C to dry mass for organic matter is assumed to be 2.5.

A.5.4.3 Other rivers

No detailed datasets were found to characterize the water quality of other river inputs included in the updated BEM. These are defined using the same concentrations as the Neponset River. According to the USGS report from Campo et al. (2003), among the 3 rivers for which extensive data are available, the Neponset median concentrations for N

and P compounds are comparable to those in other rivers (e.g., Saugus, Ipswich and Kennebec). Reported concentrations in the Charles and Merrimack rivers are higher, since these drain highly urbanized areas. Furthermore, TN and TP loads from the Kennebec River originate from similar sources to those of other rivers north of the area of interest, such as the St. John and Penobscot Rivers (i.e., forested land and agricultural sources, see Liebman et al., 2012). It is therefore reasonable to assume that these rivers have similar concentrations. For a discussion on the relevance of these rivers, see Section A.7.2.1.

A.6 Air-sea interface

A.6.1 Source of forcing

The ECMWF (European Center for Medium-range Weather Forecasting) Re-Analysis (ERA5) dataset is used as spatially and temporally varying surface forcing for all meteorological parameters: wind speed and direction, atmospheric pressure, air temperature, dew point temperature and cloud cover as well as precipitation and evaporation. The dataset is publicly available through the Climate Data Store, an online platform operated by the ECMWF: (https://cds.climate.copernicus.eu/cdsapp#!/dataset/reanalysis-era5-single-levels?tab=overview).
Additional documentation is available on the site.

This dataset has a 0.25 degrees spatial resolution and hourly temporal resolution at a global coverage and is available from 1979 onwards. The dataset is continuously updated to include newly computed months, with a delay in the order of a couple of months from real time. This spatio-temporal dataset has been transformed (in units and format) for input into BEM.

The above-mentioned wind inputs are used for the wave calculations (to compute the total bed shear stress value).

A.6.2 Parameterization of air-sea exchange

A.6.2.1 Momentum exchange

The parameters used to force the model are the wind speed and direction, as well as the atmospheric pressure. The force exerted by the wind on the water surface is coupled to the flow equations as a shear stress. To parameterize the relation between wind speed and shear stress, the aim is to be consistent with the atmospheric boundary layer model that is used in the meteorological model applied. For coupling to ERA5 this implies using a Charnock formulation (Charnock, 1995) with a time and space varying Charnock coefficient. This formulation assumes a fully developed turbulent boundary layer of the wind flow over the water surface. The associated wind speed profile follows a logarithmic shape for neutral stratification. The impact of atmospheric stability is taken into account by prescribing the *neutral* wind at 10 meters above sea-level. Such parameter is available in the ERA5 dataset.

A.6.2.2 Heat exchange

The heat exchange at the free surface between the ocean and the atmosphere is modeled by considering the separate effects of solar (shortwave) and atmospheric (longwave, downwelling) radiation, and heat loss due to back radiation (longwave, upwelling), evaporation and convection. The net solar radiation and downwelling longwave radiation are directly prescribed based on ERA5 data, while the upwelling longwave radiation is computed based on the sea surface temperature in the updated BEM. Heat losses due to evaporation and convection are functions of the wind speed. The so-called composite heat flux model (Gill,1982 and Lane,1989) is used, in which the air temperature (at 2m) and dew point temperature (at 2m) are also prescribed. For a

detailed explanation on the calculation of each of the components in the heat balance, see Chapter 11 in the Delft-3D FM User Manual (Deltares, 2019b).

A.6.2.3 Mass exchange

Precipitation and evaporation, based on ERA5, are implemented as rates (mm/day). Evaporation is prescribed as “negative precipitation” and added to the precipitation.

A.6.3 Global solar radiation

Global (shortwave) radiation is based on ERA5 in the hydrodynamic part of the updated BEM. As BLOOM uses a 24-hour time step, the daily averaged calculated global radiation at MWRA station N21 is used as input for the water quality calculations. A 3-day moving average is applied to the model input, to smooth the high-frequency variability of the model in terms of light availability, which cannot be captured by the relatively infrequent field measurements.

The model simulated daily averaged global radiation at station N21 is compared to daily averaged measurements of Photosynthetically Active Radiation (PAR) at Deer Island for validation (Figure A.6-1). The two time series are highly correlated (R=0.87). The model captures the observed seasonal and interannual variability of radiation. The shorter-term variability seems slightly underestimated by the model, for which minimum values are not as low as the measurements.

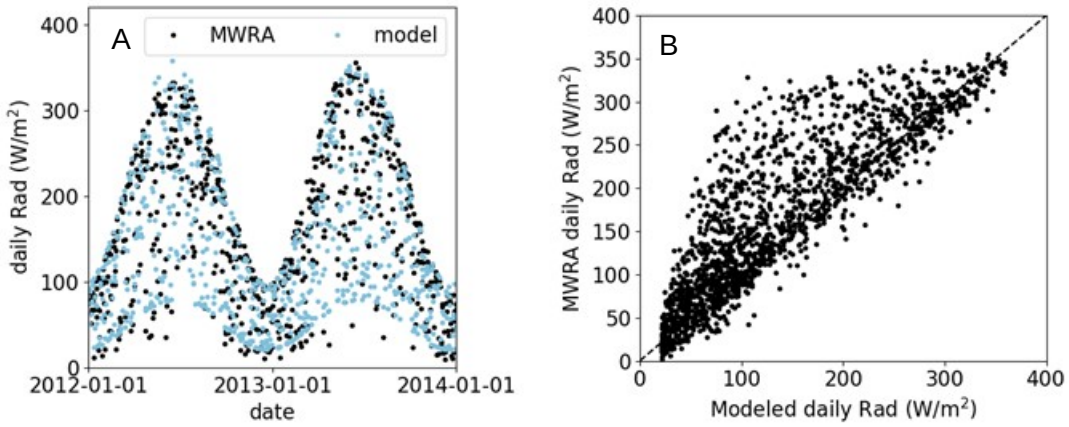

Figure A.6-1 Comparison of daily-averaged modeled and monitored radiation at Deer Island. Measured downwelling "cosine" PAR (uE/m2/s) is converted to W/m2 using a multiplication factor of 0.2174, as suggested by Chen et al. (2010). This is based on the assumption that quanta of wavelengths of 400-700 nm are equally active for photosynthesis. 550 nm (for which a mole of photons carries an energy of 2.174 105 J) is used as the typical wavelength for PAR. PAR is then converted to global radiation by dividing by 0.45 (Los, 2009). (Only 2 years are plotted in A for visualization purpose).

A.6.4 Atmospheric deposition

The model includes atmospheric deposition of nitrogen (NH4 and NO3) with constant deposition values of 10 kg N ha^{-1} yr^{-1} (6.2 10^{-4} g N m^{-2} d^{-1}) and 1.5 kg ha^{-1} yr^{-1} (3.2 10^{-4} g N m^{-2} d^{-1}) for NO3 and NH4, respectively (Townsend, 1998). These magnitudes of wet atmospheric deposition were initially reported by Lovett (1994) for the Gulf of Maine. According to Jordan and Talbot (2000), wet deposition constitutes 80-90% of the total annual atmospheric N flux to the Gulf of Maine. It is therefore assumed to be acceptable to neglect the dry deposition fraction. These values are consistent with recently reported on-land N atmospheric deposition values from the National Atmospheric Deposition Program (2019), ranging for the adjacent area approximatively 6-10 kg N ha^{1} yr^{-1}.

Atmospheric deposition of phosphorus is neglected. According to Okin et al. (2018), phosphorus deposition in the North Central Atlantic is two orders of magnitude lower than that of nitrogen deposition. Tracer simulations revealed that including this source in the updated BEM would have negligible effect on phosphorus concentrations in the area of interest.

A.7 Offshore boundary

A.7.1 Hydrodynamics

A.7.1.1 Water levels

The 2012 version of the Finite Element Solution global tidal model (FES2012) distributed by AVISO (https://www.aviso.altimetry.fr/en/data/products/auxiliary-products/global-tide-fes/description-fes2012.html) is used to force tidal water levels at the offshore boundary for the hydrodynamic component. FES2012 contains 32 tidal constituents on a 1/16° global resolution. This product is well known for its high accuracy in deep ocean and is extensively used to force tides into regional models such as the updated BEM.

The surge at the open boundaries is approximated by addition of an inverse barometer correction (IBC, Wunsch and Stammer 1997) to the astronomical water levels. This implies that the effect of wind stress is neglected locally, which is a reasonable approximation in deep water (where the boundaries are located). The IBC is a time- and space-dependent function of the local atmospheric pressure.

To account for steric (i.e. density driven) variations in water level, the daily mean water levels from the Copernicus Marine Environment Monitoring Service (CMEMS) model are used, specifically results from the “GLobal Ocean ReanalYsis and Simulation” global model product GLORYS12V1 (http://marine.copernicus.eu/services-portfolio/access-to-products/?option=com_csw&view=details&product_id=GLOBAL_REANALYSIS_PHY_001_030).

A.7.1.2 Salinity and temperature

Daily vertical profiles for salinity and temperature from CMEMS are used to force the BEM model boundaries, specifically results from the global model product GLORYS12V1. An example of this product is shown in Figure A.7-1 for surface salinity. This product is a global ocean eddy-resolving reanalysis product, with a horizontal resolution of 1/12° and 50 vertical levels. The model platform used to prepare this product is “NEMO” (Nucleus for European Modelling of the Ocean), an open source, community ocean model (Gurvan et al. 2017). For the CMEMS global model product, NEMO uses meteorological forcing from ECMWF, specifically the “ERA-Interim” a global atmospheric data reanalysis dataset (Berrisford et al., 2011; Dee et al., 2011). Meteorological observations are assimilated by means of a reduced-order Kalman filter. Along track altimeter data (Sea Level Anomaly), satellite Sea Surface Temperature, Sea Ice Concentration and in situ temperature and salinity vertical profiles are jointly assimilated. Moreover, a three-dimensional variation assimilation (3D-VAR) scheme provides a correction for the slowly-evolving large-scale biases in temperature and salinity. More details about the GLORYS12V1 global model product characteristics and quality are provided by CMEMS (see http://resources.marine.copernicus.eu/documents/QUID/CMEMS-GLO-QUID-001-030.pdf)

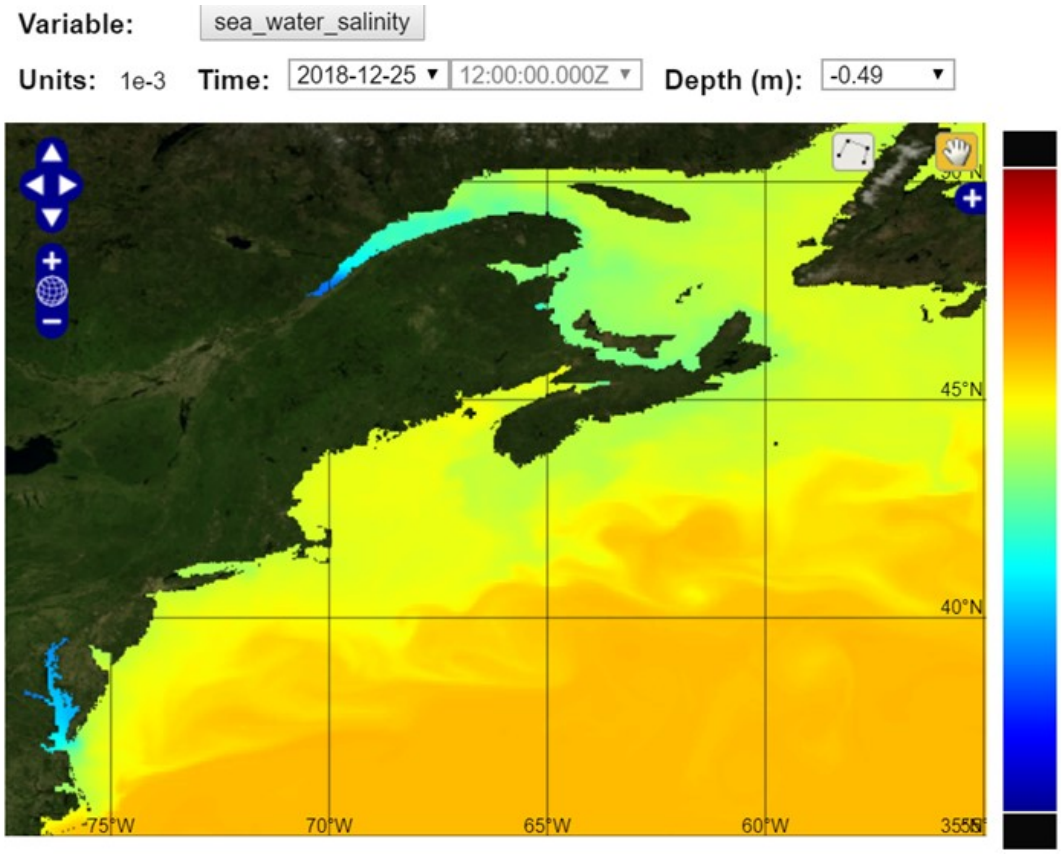

Figure A.7-1 CMEMS web viewer for GLORYS12V1 product which is used to define the boundary conditions of temperature and salinity for the updated BEM: example for surface salinity. (This image is from a website viewer that does not offer perceptually uniform or colorblind-optimal color maps).

A.7.2 Water quality

A.7.2.1 Approach

According to Zhang et al. (2019) the nitrogen budget for the Gulf of Maine (GoM) is dominated by exchange fluxes between open ocean waters and the GoM. Coastal sources constitute about 4% of influxes. For the smaller domain of the former BEM (Figure A.7-2), Zhao et al. (2017) cite Hunt et al. (1999) suggesting that 7% of influxes is from coastal sources and atmospheric deposition and the remaining 93% from the GoM.

The updated BEM water quality model has a much larger domain than the former BEM. The ambition is not to provide a realistic water quality model for the complete domain, but to provide a realistic estimate of the quality of the GoM waters entering Massachusetts Bay. It should be noted that by simulating water quality on the larger domain, the variable influence of the inflow of Merrimack River into Mass Bay is resolved.

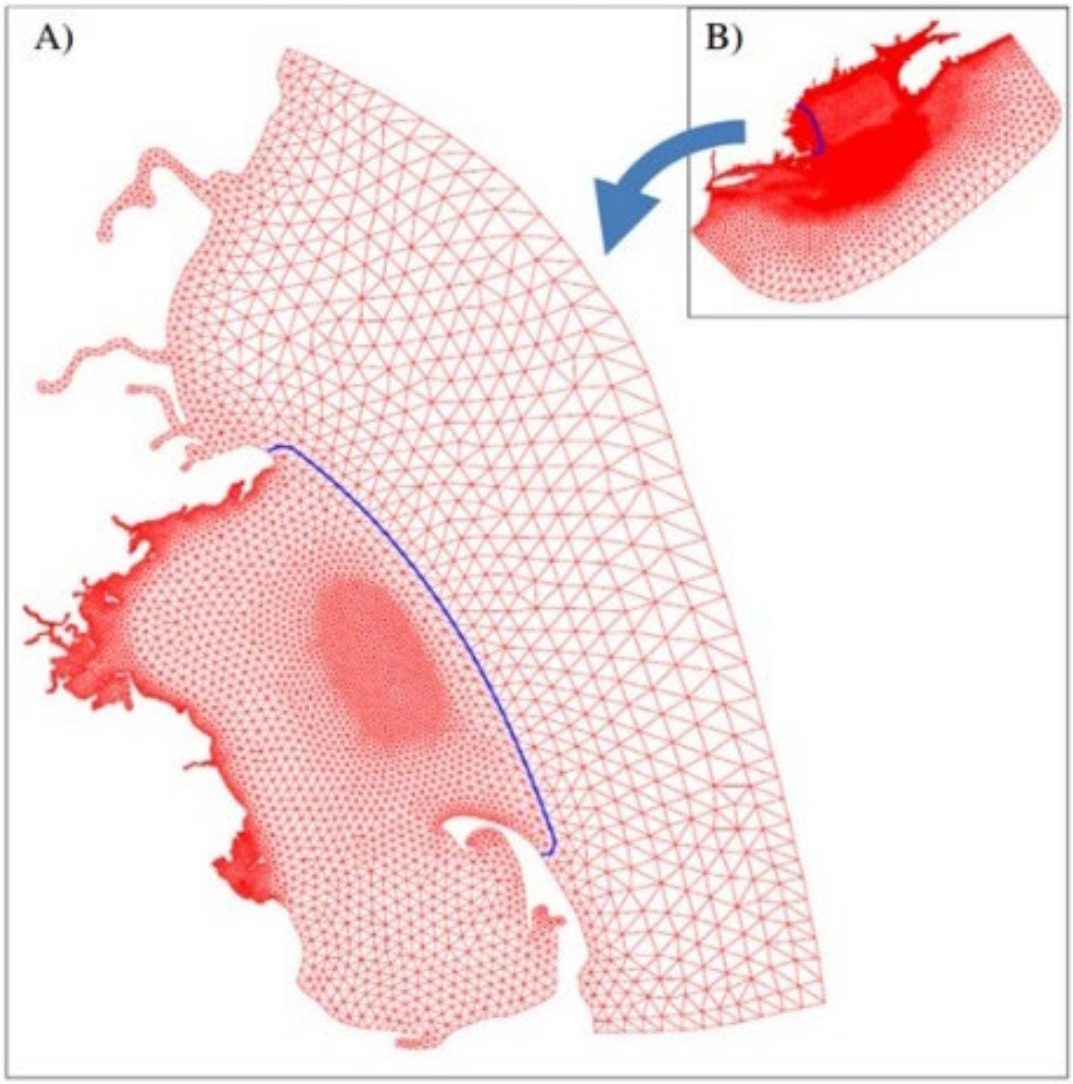

Figure A.7-2 Domain of the former BEM water quality model, indicated by the area west of the blue line (copied from Xue et al., 2014).

The updated BEM is nested in a global model for providing hindcasts of water quality. This global model is able to provide realistic time variable data for the quality of ocean waters as affected by larger scale ocean dynamics.

The results by Zhang et al. (2019) indicate that the relevance of riverine inputs away from the direct area of interest is expected to be limited. For this reason, the lack of concentration data for far away rivers is not considered to be a problem for the updated BEM.

A.7.2.2 Source of forcing

Water quality offshore boundary conditions are defined using the CMEMS Global Ocean Biogeochemistry Hindcast (http://marine.copernicus.eu/services-portfolio/access-to-products/?option=com_csw&view=details&product_id=GLOBAL_REANALYSIS_BIO_001_029). This product provides three dimensional biogeochemical daily or monthly fields since 1993 at a ¼-degree spatial resolution, and on 75 different vertical levels. It is produced with the Pelagic Interactions Scheme for Carbon and Ecosystem Studies (PISCES) biogeochemical model, from the NEMO platform (https://www.nemo-ocean.eu/), and without data assimilation. The dataset includes fields for seawater concentrations of nitrate (NO_3), phosphate (PO_4), silicate (Si), dissolved oxygen (O_2), as well as Chl-a and PHYC (carbon contained in phytoplankton) that can be used as a proxy for organic matter concentrations. To limit the size of the boundary input file, CMEMS monthly outputs are used. An example of this product is shown in Figure A.7-3 for nitrate. The conversion factors for transforming CMEMS output to BEM modeled substances are summarized in Table A.7-1.

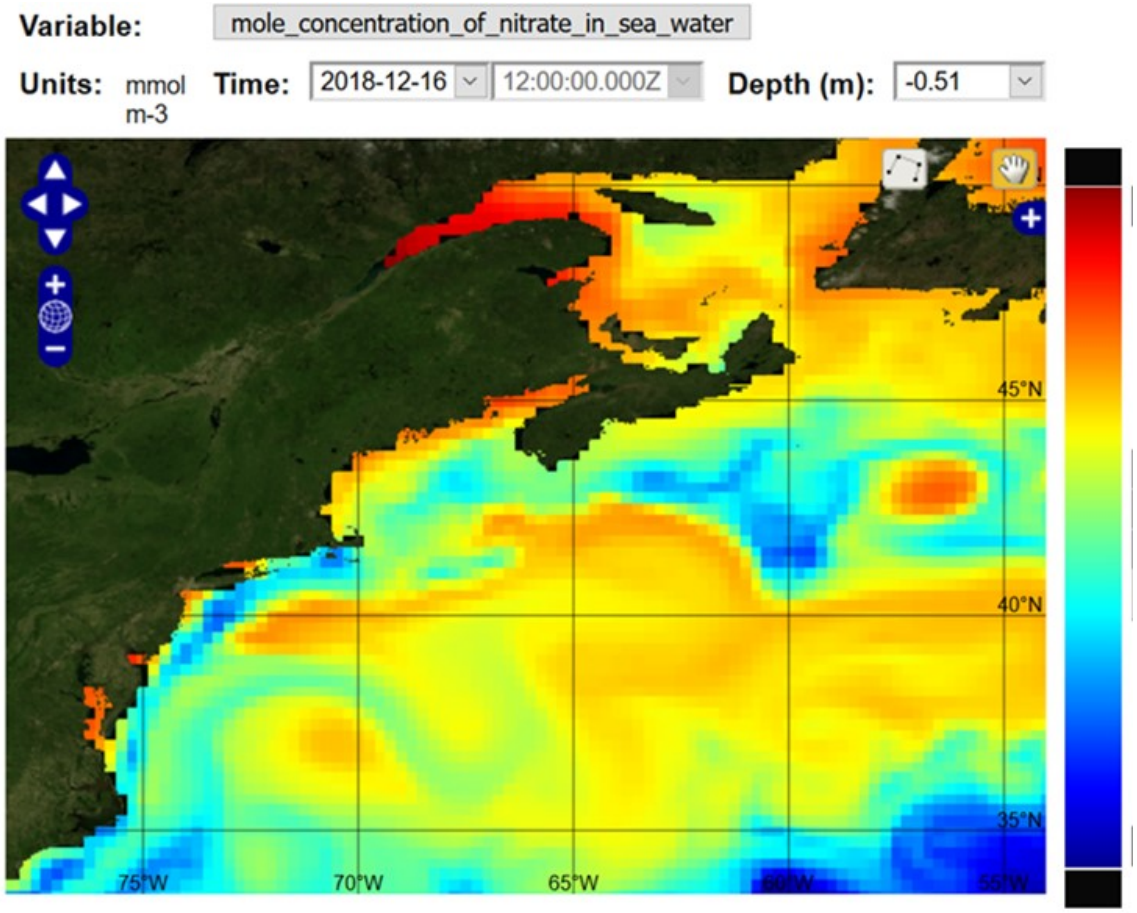

Figure A.7-3 CMEMS web viewer for Global Ocean biogeochemistry product, which is used to provide boundary conditions for the updated BEM water quality component: example for nitrate. (This image is from a website viewer that does not offer perceptually uniform or colorblind-optimal color maps).

Table A.7-1 Conversion factors for CMEMS output parameters to BEM modeled substances for the definition of the offshore boundary.

State variable	Descriptive Name	CMEMS output (offshore boundary)
OXY	Oxygen	CMEMS output O_2
POC1	Particulate Organic Carbon	CMEMS output PHYC * 2 (**note 1**)
DOC	Dissolved Organic Carbon	(199/20) × (12/16) × PON1 (**note 2**)
PON1	Particulate Organic Nitrogen	POC1 * 16/106 * 1.15 **(notes 3, 4**)
DON	Dissolved Organic Nitrogen	1.15 * 3.24 × PON1 (**notes 4, 5**)
NH4	Ammonium	0.0
NO3	Nitrate	CMEMS output NO_3 * 1.15 (**note 4**)
POP1	Particulate Organic Phosphorus	POC1 / 106 (**note 3**)
DOP	Dissolved Organic Phosphorus	1.0 × POP1 (**note 6**)
PO4	Phosphate	CMEMS output PO_4
Si	Silica	CMEMS output Si
Opal	Opal	POC1 * 0.5 * 0.13 (**note 7**)
IM1	Inorganic suspended Matter	0.0
Phyto-plankton	phytoplankton	0.0

1 It is assumed that the detritus to algae ratio (both expressed as C) is 2.

2 199:20 is DOM mineralization C:N stoichiometry (Hopkinson and Vallino, 2005).

3 PON and POP use molar Redfield C:N:P ratio 106:16:1 (Redfield, 1934).

4 A scaling factor of 1.15 is needed to reproduce near surface values during periods of stratification at the most offshore monitoring station (i.e., F22). This scaling factor accounts for differences between the updated model and the CMEMS model with respect to river and atmospheric loads for the full domain of the model; and any differences between CMEMS simulated concentrations in GoM and observations. See Appendix B (model calibration) for more details.

5 The proportion of DON:PON is determined based on measurements at MWRA monitoring station F10 (most saline station where it is possible to calculate DON), at dates where TDN, NH4, (NO3+NO2) and PON measurements are available. At each sampling date, DON=MAX(TDN-NH4-(NO3+NO2), 0.), see Figure A.7-4. The average DON:PON ratio for 2012-2016 is 3.24.

6 Similarly, at each sampling date where TDP, PO4 and PP are measured, DOP is calculated as: DOP=MAX(TDP-PO4, 0.), see Figure A.7-4. The average DOP:PP ratio for 2012-2016 is 1.0.

7 Opal is estimated using the C:Si ratio for diatoms from Brzezinski (1985) and assuming that half of the phytoplankton carbon biomass is constituted by diatoms.

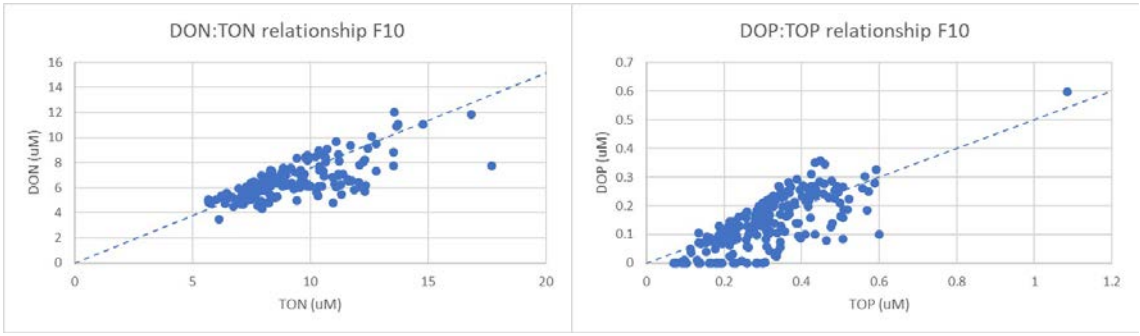

Figure A.7-4 Relation between the dissolved and total organic pools of nitrogen and phosphorus derived from analysis results from MWRA station F10. The dashed lines represent DON:TON=0.76 and DOP:TOP=0.5.

A.8 Other features

A.8.1 Amount of fine inorganic particles available for resuspension

The fraction of fine particles in bed sediment is forced spatially using data from "usSEABED", an extensive database of seafloor characteristics compiled by USGS and numerous partner organizations, for the U.S. Atlantic Coast (Reid et al., 2005; https://pubs.usgs.gov/ds/2005/118/). This database contains particle size data at more than 49,000 locations. Within the domain of interest, data are available at over 22,000 locations (Figure A.8-1, left). The data include information on latitude, longitude, and percentages of clay, mud (i.e., clay+silt), and sand fractions.

A constant 10 cm sediment layer is assumed everywhere, with a porosity of 0.4 and a sediment density of 2000 kg/m^3). Within this sediment layer, the fraction of fine inorganic particles available for resuspension is defined using the mud proportion. Data are spatially interpolated over the model grid for calculations. To be sure that the whole grid is covered, 4 points are added at the domain limits with a fraction of fines of 10%.

The proportion of fines in bed sediment is extremely variable over the domain, ranging from 0 to 100% (median=9%). When zooming in around the area of interest (Figure A.8-1, right), the variability stays comparably high, with proportions of fines ranging from 0 to 100% (median=10%) over the 5628 documented locations.

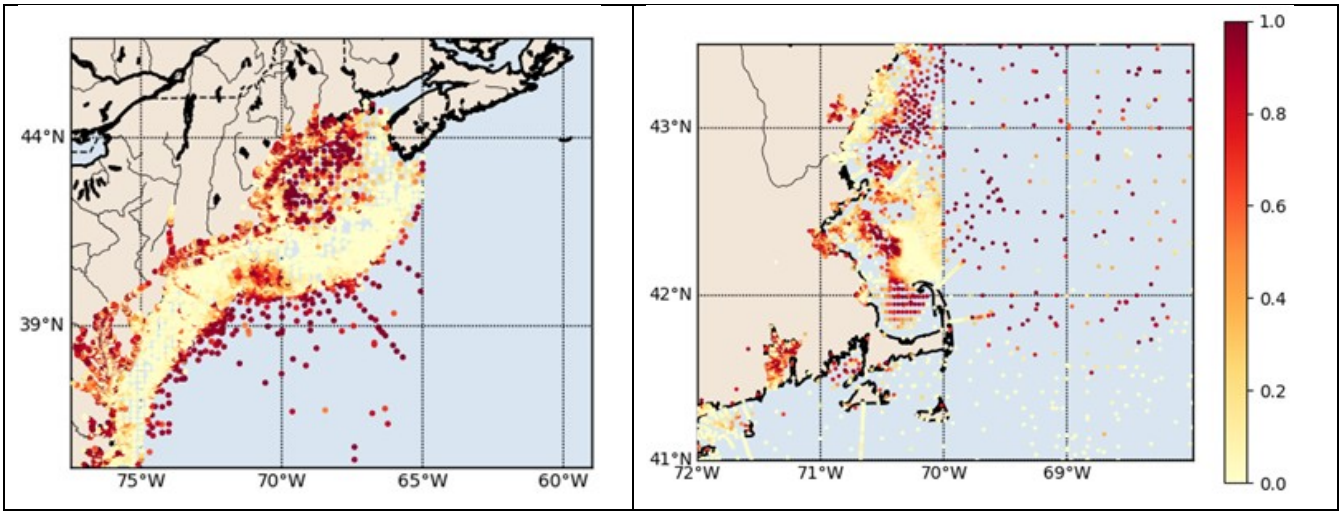

Figure A.8-1: Fraction of fines (mud) in bed sediment. Full domain (left), zoom (right).

This dataset was included in the study from the Massachusetts Division of Marine Fisheries (Ford and Voss, 2010) on seafloor composition in Massachusetts waters. The latter analysis shows that the seafloor composition is extremely patchy; 21% of the study area is muddy, and therefore prone to be highly erodible.

A.8.2 Additional loads for water quality component

In addition to river loads, the MWRA outfall and atmospheric deposition, a number of other potential carbon or nutrient loads to Massachusetts Bay and the model domain

include: Non-MWRA outfalls, Non-point source runoff, and Combined Sewer Overflows (CSOs) in Boston Harbor. *None* of these additional nutrient sources is included. While the former BEM did include CSOs in Boston Harbor, it did not include the other sources (Zhao et al., 2017 and references therein). Based on information provided by MWRA, Boston Harbor CSOs have decreased significantly since the 1990s. Only the MWRA outfall is included in the updated BEM as the model focus does not extend to potential effects of other outfalls.

A.8.3 Initial conditions

For temperature and salinity, the updated BEM is initialized to the GLORYS12V1 3D temperature and salinity fields. These are automatically interpolated to the model grid in the horizontal and vertical. These values are consistent with what is prescribed at the open boundaries (see Section A.6.1). For nutrient and other water quality parameters the initial conditions are defined using 2D depth-averaged fields from the CMEMS Global Ocean Biogeochemistry Hindcast, which is also used to prescribe the open boundaries (Section A.6.2). The conversion factors for transforming CMEMS output to modeled substances are summarized in Table A.7-1.

The prescribed initial conditions are not considered to be critical for the BEM model results as the model is run with a spin-up period of approximately one year (as explained in Appendix B on calibrations).

A.9 References

Alber, M. and A. Chan, 1994. Sources of contaminants to Boston Harbor: revised loading estimates. Boston: Massachusetts Water Resources Authority. Report 1994-01. 93pp. http://www.mwra.state.ma.us/harbor/enquad/pdf/1994-01.pdf

Berrisford, P., Dee, D., Poli, P., Brugge, R., Fielding, K., Fuentes, M., Kallberg, P., Kobayashi, S., Uppala, S. and Simmons, A., 2011. The ERA-Interim archive, version 2.0. ERA report, series. 1. Technical Report. ECMWF pp23.

Blauw, A.N., H.F.J. Los, M. Bokhorst and P.L.A. Erftemeijer, 2009. GEM: a Generic Ecological Model for estuaries and coastal waters. Hydrobiologia 618: 175-198.

Bridges, T. and I. Dombroski, 2018. Lower Merrimack River Monitoring Project Summer/Fall 2017. EPA Report EMT-2017-MERR.

Brzezinski, MA, 1985. The Si:C:N ratio of marine diatoms: interspecific variability and the effect of some environmental variables. Journal of Phycology 21(3), 1985: 347-357.

Campo, KW, SM Flanagan, KW Robinson, 2003. Water quality of selected rivers in the New England coastal basins in Maine, Massachussetts, New Hampshire and Rhode Island, 1998-2000. U.S. Geological Survey, Water-Resources Investigations Report 03-4210. *https://pubs.usgs.gov/wri/wri034210/wrir034210report.pdf*.

Chapra, S.C., 1996. Surface Water Quality Modeling. New York: McGraw-Hill Science / Engineering / Math.

Charnock, H. (1955). Wind stress on a water surface. Quarterly Journal of the Royal Meteorological Society, 81(350), 639-640.

Dawson, C., & Mirabito, C. M. (2008). The shallow water equations. University of Texas, Austin, 29.

D. P. Dee, S. M. Uppala, A. J. Simmons, P. Berrisford, P. Poli, S. Kobayashi, U. Andrae, M.A. Balmaseda, G. Balsamo, P.Bauer, P.Bechtold, A. C. M. Beljaars, L. van de Berg, J. Bidlot, N. Bormann, C. Delsol, R. Dragani, M. Fuentes, A. J. Geer, L. Haimberger, S. B. Healy, H. Hersbach, E. V. Hólm, L. Isaksen, P. Kållberg, M. Köhler, M. Matricardi, A. P. McNally, B. M. Monge-Sanz, J.-J. Morcrette, B.-K. Park, C. Peubey, P. de Rosnay, C. Tavolato, J.-N. Thépaut, F. Vitart, 2011. The ERA-Interim reanalysis: configuration and performance of the data assimilation system. Quarterly Journal of the Royal Meteorological Society, 137, 656, *https://doi.org/10.1002/qj.828*.

Deltares, 2014. Processes Library Description. Version: 5.01 Revision 34078, Delft, The Netherlands.

Deltares, 2019a. D-Flow Flexible Mesh, Technical Reference Manual. Released for: Delft3D FM Suite 2020. Version: 1.1.0 SVN Revision: 63652. December 4, 2019.

Deltares. 2019b. Delft3D Flexible Mesh Suite, D-Flow FM in Delta Shell, User Manual, Version 1.5.0, December 5, 2019 (*https://content.oss.deltares.nl/delft3d/manuals/D-Flow_FM_User_Manual.pdf*)

Deltares, 2020. Delft3D Flexible Mesh Suite, D-Water Quality Process Library Description, Technical Reference Manual. Version 5.01 SVN Revision: 64968. February 1, 2020 (https://content.oss.deltares.nl/delft3d/manuals/D-Water_Quality_Processes_Technical_Reference_Manual.pdf)

ESRLAC, 2012. Exeter-Squamscott River Watershed Management Plan Update. Exeter-Squamscott River Local Advisory Committee. Accessed online Jan 10, 2020. *https://www.des.nh.gov/organization/divisions/water/wmb/rivers/documents/ext-squam-plan.pdf*

Ford, KH, S Voss, 2010. Seafloor sediment composition in Massachusetts determined using point data. Massachusetts Division of Marine Fisheries Technical Report TR-45.

Gill, A. E. (1982). Atmosphere-Ocean dynamics (International Geophysics Series). academic press.

Gurvan, Madec, Romain Bourdallé-Badie, Pierre-Antoine Bouttier, Clément Bricaud, Diego Bruciaferri; Daley Calvert, Jérôme Chanut, Emanuela Clementi, Andrew Coward, Damiano Delrosso, Christian Ethé, Simona Flavoni, Tim Graham, James Harle, Doroteaciro Iovino, Dan Lea, Claire Lévy, Tomas Lovato, Nicolas Martin, Sébastien Masson, Silvia Mocavero, Julien Paul, Clément Rousset, Dave Storkey, Andrea Storto, Martin Vancoppenolle, 2017. NEMO ocean engine (Version v3.6-patch). Notes Du Pôle De Modélisation De L'institut Pierre-simon Laplace (IPSL). Zenodo. http://doi.org/10.5281/zenodo.3248739

Hunt, C.D., Kropp, R.K., Fitzpatrick, J.J., Yodzis, P, Ulanowicz R.E., 1999. A review of issues related to the development of a food web model for important prey of endangered species in Massachusetts and Cape Cod Bays. Boston: Massachusetts Water Resources Authority. Report 1999-14. 62 p.

Hurdle, D. P., & Stive, R. J. H. (1989). Revision of SPM 1984 wave hindcast model to avoid inconsistencies in engineering applications. Coastal Engineering, 12(4), 339-351.

HydroQual and Normandeau. 1995. A water quality model for Massachusetts and Cape Cod Bays: Calibration of the Bays Eutrophication Model (BEM). Boston: Massachusetts Water Resources Authority. Report 1995-08. 402 p. *http://www.mwra.state.ma.us/harbor/enquad/pdf/1995-08.pdf*

Jordan, C.E. and Talbot, R.W., 2000. Direct atmospheric deposition of water-soluble nitrogen to the Gulf of Maine. Global Biogeochemical Cycles 14(4), 2000: 1315-1329.

Lane, A. (1989). The heat balance of the North Sea, Proudman Oceanographic Laboratory, Report No. 8.

Liebman, M, JS Latimer, S Bricker, 2012. Eutrophication, state of the Gulf of Maine report. Gulf of Maine Council on the Marine Environment, June 2012. http://www.gulfofmaine.org/2/wp-content/uploads/2014/03/eutrophication.pdf.

Los, F.J., Villars, M.T., Van der Tol, M.W.M., 2008. A 3-dimensional primary production model (BLOOM/GEM) and its applications to the (southern) North Sea (coupled physical-chemical-ecological model). Journal of Marine Systems, 74 (1-2): 259-294. https://doi.org/10.1016/j.jmarsys.2008.01.002

Los, F.J., 2009. Eco-hydrodynamic modeling of primary production in coastal waters and lakes using BLOOM. Ph.D. Thesis, Wageningen University, 2009.

Maguire, T. J., & Fulweiler, R. W. (2017). The fate and effect of dissolved silicon within wastewater treatment effluent. Environmental Science & Technology, 51(13): 7403-7411. DOI: 10.1021/acs.est.7b01276

Meybeck, M, 1982. Carbon, nitrogen, and phosphorus transport by world rivers. Am J Sci 282, 1982: 401-450.

National Atmospheric Deposition Program, 2019. 2017 Total Deposition Measurement Model Fusion Maps. Wisconsin State Laboratory of Hygiene, University of Wisconsin, Madison, WI. Accessed online 2/3/2020: http://nadp.slh.wisc.edu/committees/tdep/reports/TDEP_report_2017.pdf

NH DES, 2019a. The Isinglass River Environmental Fact Sheet. New Hampshire Department of Environmental Services. Accessed online Jan 10, 2020. https://www.des.nh.gov/organization/commissioner/pip/factsheets/rl/documents/rl-18.pdf

NH DES, 2019b. The Lamprey River Watershed Environmental Fact Sheet. New Hampshire Department of Environmental Services. Accessed online Jan 10, 2020. https://www.des.nh.gov/organization/commissioner/pip/factsheets/rl/documents/rl-7.pdf

Okin, GS, Baker, AR, Tegen, I, Mahowald, NM, Dentener, FJ, Duce, RA, Galloway, JN, Hunter, K, Kanakidou, M, Kubilay, N, Prospero, JM, Sarin, M., Surapipith, V, Uematsu, M and T Zhu, 2011. Impacts of atmospheric nutrient deposition on marine productivity: Roles of nitrogen, phosphorus, and iron. Global Biogeochemical Cycles 25, GB2022.

PREP, 2012. Watershed Poster. Piscataqua Regional Estuaries Partnership. Accessed online Jan 10, 2020. http://prepestuaries.org/01/wp-content/uploads/2013/02/2012_Watershed_Poster.pdf

Redfield, AC, 1934. On the proportions of organic derivatives in sea water and their relation to the composition of plankton. James Johnston Memorial Volume 176.

Reid, JM, JA Reid, CJ Jenkins, ME Hastings, SJ Williams, LJ Poppe, 2005. usSEABED: Atlantic Coast Offshore Surficial Sediment Data Release. U.S. Geological Survey, Coastal and Marine Geology Platform.

Smagorinsky, J. (1963). General circulation experiments with the primitive equations: I. The basic experiment. Monthly weather review, 91(3), 99-164.

Smits, J.G.C. and J.K.L. van Beek, 2013. ECO: A Generic Eutrophication Model Including Comprehensive Sediment-Water Interaction. PLoS ONE 8(7), 2013: e68104.

Swart, 1974. Offshore sediment transport and equilibrium beach profiles. Ph.D. thesis, DelftUniversity of Technology, Delft, The Netherlands. Delft Hydraulics Publ. 131.

Thomann, R.V. and J.A. Mueller, 1987. Principles of Surface Water Quality Modeling and Control. New York: Harper & Row Publ., 1987.

Townsend, D.W., 1998. Sources and cycling of nitrogen in the Gulf of Maine. Journal of Marine Systems 16, 1998: 283-295.

Uittenbogaard, R. E., Van Kester, J. A. T. M., & Stelling, G. S. (1992). Implementation of three turbulence models in 3D-TRISULA for rectangular grids. Report Z81, Delft Hydraulics.

Unesco, I., & SCOR, I. (1981). Background papers and supporting data on the international equation of state of seawater 1980.

Van Gils, J, K van Heeringen, D Schwanenberg, E de Goede and F Zijl, 2007. Pearl River Delta Water Quality Model. Final Study Report, Delft: Delft Hydraulics, 2007.

Wunsch, C., & Stammer, D. (1997). Atmospheric loading and the oceanic “inverted barometer” effect. Reviews of Geophysics, 35(1), 79-107.

Zhang, S., Stock, C.A., Curchitser, E.N., Dussin, R., 2019. A numerical model analysis of the mean and seasonal nitrogen budget on the Northeast U.S. Shelf. Journal of Geophysical Research: Oceans, 124, 2969–2991. https://doi.org/ 10.1029/2018JC014308

Zhao L, Beardsley RC, Chen C, Codiga DL, Wang L. 2017. Simulations of 2016 Hydrodynamics and Water Quality in the Massachusetts Bay System using the Bays Eutrophication Model. Boston: Massachusetts Water Resources Authority. Report 2017-13. 111pp.

Appendix A1. Hydrodynamic equations

D-Flow FM solves the so-called shallow water equations (SWE) for incompressible flow (Dawson and Mirabito, 2008) which are described by the following continuity and momentum equations:

$$\frac{\partial \mathrm{h}}{\partial \mathrm{t}} + \frac{\partial \mathrm{uh}}{\partial \mathrm{x}} + \frac{\partial \mathrm{vh}}{\partial \mathrm{y}} + \frac{\partial \mathrm{w}}{\partial \mathrm{z}} = \mathrm{hQ}$$

$$\frac{\partial \mathrm{u}}{\partial \mathrm{t}} + \mathrm{u}\frac{\partial \mathrm{u}}{\partial \mathrm{x}} + \mathrm{v}\frac{\partial \mathrm{u}}{\partial \mathrm{y}} + \mathrm{w}\frac{\partial \mathrm{u}}{\partial \mathrm{z}} - \mathrm{fv} = -\frac{1}{\rho_0}\frac{\partial \mathrm{P}}{\partial \mathrm{x}} + F_x + \frac{1}{\partial \mathrm{z}}\left(\nu_v \frac{\partial \mathrm{u}}{\partial \mathrm{z}}\right) + M_x$$

$$\frac{\partial \mathrm{v}}{\partial \mathrm{t}} + \mathrm{u}\frac{\partial \mathrm{v}}{\partial \mathrm{x}} + \mathrm{v}\frac{\partial \mathrm{v}}{\partial \mathrm{y}} + \mathrm{w}\frac{\partial \mathrm{v}}{\partial \mathrm{z}} + \mathrm{fu} = -\frac{1}{\rho_0}\frac{\partial \mathrm{P}}{\partial \mathrm{y}} + F_y + \frac{1}{\partial \mathrm{z}}\left(\nu_v \frac{\partial \mathrm{v}}{\partial \mathrm{z}}\right) + M_y$$

Where u and v are the depth averaged velocities, h is the local total water depth, Q is the contributions per unit area due to discharge or withdrawal of water, precipitation and evaporation, ν_v is the vertical eddy viscosity coefficient and f is the Coriolis force. Within the SWE, the vertical momentum equation is reduced to a hydrostatic pressure equation. The vertical velocity w is computed from the continuity equation and may be interpreted as the velocity associated with up- or downwelling motions.

Density variations are neglected, except in the baroclinic pressure terms. ∂P/∂x and ∂P/∂y represent the pressure gradients, which comprise the barotropic pressure gradient (gradients of the free surface level, including atmospheric pressure effects) and the baroclinic pressure gradients, which arise from depth-integrated horizontal differences in density and the hydrostatic pressure assumption. In this term, the density is calculated from the local temperature and salinity through the equation of state, in this case UNESCO formulation y (UNESCO, 1981a).

The forces F_x and F_y in the momentum equations represent the imbalance of horizontal Reynolds stresses. The 2D turbulence component is introduced through the horizontal viscosity and eddy diffusivity coefficients, which are determined using the Smagorinsky model for sub-grid scale turbulence (Smagorinsky, 1963). The vertical turbulence is introduced through a two-equation turbulence closure model called $k - \varepsilon$, which determines the vertical viscosity and eddy diffusivity coefficients. For more details we refer to Uittenbogaard et al. 1992.

M_x and M_y represent the contributions due to external sources or sinks of momentum (external forces by hydraulic structures, wave stresses, etc). In the BEM model, wind stress in introduced through this term.

Additional details about the hydrodynamic modeling software can be found in Deltares, 2019a, b.

Appendix A2. Water quality equations

A2.1. Basic equations

The water quality (WQ) component solves the transport equation or advection-diffusion equation:

$$\frac{\partial C}{\partial t} = \frac{\partial}{\partial x}\left(K_x \frac{\partial C}{\partial x}\right) - u\frac{\partial C}{\partial x} + \frac{\partial}{\partial y}\left(K_y \frac{\partial C}{\partial y}\right) - v\frac{\partial C}{\partial y} + \frac{\partial}{\partial z}\left(K_z \frac{\partial C}{\partial z}\right) - w\frac{\partial C}{\partial z} + S$$

where:

C	g/m^3	Concentration
K_x, K_y, K_z	m^2/s	dispersion coefficients in three directions
S	g/m^3/s	source term
u,v,w	m/s	velocity components in three directions
x,y,z	m	spatial co-ordinates

The source term S represents the substance-specific behaviour (decay, sedimentation and resuspension, reaeration, etc.; see next section below on Process Equations). The above equation is also solved by the hydrodynamic component, for the state variables salinity and temperature. These two state variables affect the water density and therefore the pressure gradient terms in the momentum equations.

A2.2. Process equations

Symbols used are defined and explained in Section A2.3 below. In the following, POX refers to particulate organic X, and DOX refers to dissolved organic X, where X is C (carbon), N (nitrogen), or P (phosphorous).

Balance equations for state variables (terms S of equation in A2.1)

$$\frac{dNO_3}{dt} = nit - den - upt_N * (1 - f_{am})$$

$$\frac{dNH_4}{dt} = \left(1 - b_{pocdoc}\right) * dec_{PON} - nit + dec_{PON_S} + f_{aut} * mor_N - upt_N * f_{am}$$

$$\frac{dPO_4}{dt} = \left(1 - b_{pocdoc}\right) * dec_{POP} + dec_{POP_S} + f_{aut} * mor_P - upt_P$$

$$\frac{dSi}{dt} = dis_{BSi} + dis_{BSi_S} + f_{aut} * mor_{Si} - upt_{Si}$$

$$\frac{dALG_i}{dt} = gro_i - mrt_i - sed_i$$

$$\frac{dO_2}{dt} = rea + \left(gro_C - dec_{POC} - dec_{PO_{CS}}\right) * s_o + (upt_N * (1 - f_{am}) - nit) * s_{no}$$

$$\frac{dPOX}{dt} = mor_X * (1 - f_{aut}) - sed_{POX} - dec_{POX} + res_{POXS} \quad X = C, N, P$$

$$\frac{dDOX}{dt} = b\_pocdoc * dec_{POX} - dec_{DOX} \quad X = C, N, P$$

$$\frac{dPOXS}{dt} = (sed_{POX} - dec_{POXS} - bur_{POXS} - res_{POXS}) * Z \qquad X = C, N, P$$

$$\frac{dBSi}{dt} = mor_{Si} * (1 - f_{aut}) - sed_{BSi} - dis_{BSi} + res_{BSiS}$$

$$\frac{dBSiS}{dt} = (sed_{BSi} - dis_{BSiS} - bur_{BSiS} - res_{BSiS}) * Z$$

where:

i = algae species phenotypes

$$upt_X = \sum_{i=1}^{n} (gro_i * s_{X,i})$$

$$mor_X = \sum_{i=1}^{n} (mrt_i * s_{X,i})$$

X = element carbon, nitrogen, phosphorus and silicate

$$f_{am} = \frac{\mathrm{MIN}(NH_4, upt_N * \Delta t)}{upt_N * \Delta t}$$

Phytoplankton processes

$$gro_i = \frac{ALG_{i,new} - ALG_i}{\Delta t} + mrt_i$$

$$mrt_i = m_i * ALG_i$$

$$p_i = p_{i,0} * (T - kt_{p,i})$$

$$r_i = r_{i,0} * kt_{r,i}^{\ T}$$

$$pg_i = p_i + r_i$$

$$m_i = m_{i,0} * kt_{m,i}^{\ T}$$

Optimization: find set of new concentrations of ALG_i with maximum:

$$\sum_{i=1}^{n} (pg_i * le_i - r_i) * ALG_i$$

satisfying the following constraints:

$$\sum_{i=1}^{3} ALG_{i,new} \leq \sum_{i=1}^{3} (ALG_i)\, e^{(pg_i * le_i - r_i) * \Delta t}$$ *(growth constraint per species group)*

$$\sum_{i=1}^{3} ALG_{i,new} \geq \sum_{i=1}^{3} ALG_i * e^{-m_i * \Delta t}$$ *(mortality constraint per species group)*

$$\sum_{i=1}^{n} (s_{N,i} * ALG_{i,new}) \leq \sum_{i=1}^{n} (s_{N,i} * ALG_i) + NO_3 + NH_4$$ *(nutrient constraint, nitrogen)*

$$\sum_{i=1}^{n} (s_{P,i} * ALG_{i,new}) \leq \sum_{i=1}^{n} (s_{P,i} * ALG_i) + PO_4$$ *(nutrient constraint, phosphorus)*

$$\sum_{i=1}^{n} (s_{Si,i} * ALG_{i,new}) \leq \sum_{i=1}^{n} (s_{Si,i} * ALG_i) + Si$$ *(nutrient constraint, silicate)*

$$k_{min,i} \leq k_d \leq k_{max,i}$$ *(light constraint)*

where:

$$k_{\max,i} = f_{table}(le_{cr})$$

$$le_{cr} = \frac{m_i + r_i}{pg_i}$$

Extinction of light

$$k_d = k_b + k_{IM} + k_{POM} + k_{ALG} + k_{DOM}$$
$$k_{POM} = e_{POC} * POC$$
$$k_{ALG} = \sum_{i=1}^{n} (e_{ALGi} * ALG_i)$$
$$k_{IM} = e_{IM} * IM$$
$$k_{DOM} = e_{DOC} * DOC$$

Decomposition of organic matter, dissolution of biogenic silica

$$dec_{POX} = (f_{T,dec} * k_{decL,POX} + (k_{decH,POX} - k_{decL,POX}) * f_{nut}) * POX$$ *(X = C, N, P)*

$$dec_{DOX} = f_{T,dec} * k_{decDOC} * DOX$$

$$dis_{BSi} = f_{T,dis} * k_{dis,BSi} * BSi * (Si_{eq} - Si)$$

$$dec_{POXS} = \frac{k_{dec,POXS} * f_{T,dec} * POXS}{Z}$$

$$dis_{BSiS} = \frac{k_{dis,BSiS} * f_{T,dis} * BSiS}{Z}$$

where:

$f_{T,pr} = kt_{pr}^{(T-20)}$ *where: pr = dec, den, nit, dis*

$$f_{nut} = \text{MIN}(\frac{PON / POC) - sl_N}{su_N - sl_N}, \frac{POP / POC) - sl_P}{su_P - sl_P})$$

Nitrification and denitrification

$$nit = k_{nit} * NH_4 * f_{T,nit}$$

$$den = \frac{k_{den} * NO_3 * f_{T,den}}{Z}$$

The process *den* represents sediment denitrification and is therefore restricted to the lower layer. Denitrification can occur in the water column under low oxygen conditions. For details see Deltares (2020).

Reaeration

$$rea = (0.3 + 0.028 * W^2) * \frac{(O_{2,eq} - O_2)}{Z} * k_{rea}$$

where:

$$O_{2,eq} = (1 - cl)/10^5 * [14.652 - 0.41022 * T + (0.089392 * T)^2 - (0.042685 * T)^3]$$

$$cl = \frac{SAL}{1.805} * \left[1000. + 0.7 * \frac{SAL}{1. - SAL/1000.} - 0.0061 * (T - 4.)^2\right]$$

Sedimentation

$sed_Y = \frac{v_Y * Y}{Z}$ *where: Y = ALGi, POX, BSi*

Resuspension

$res_Y = F_{res} \frac{Y}{DMS} \frac{1}{Z}$ *where: Y = POX$_S$, BSi$_S$*

$F_{res} = Z_{res} \left(\frac{\tau_{flow} + \tau_{waves}}{\tau_{cr,res}} - 1\right)$

Z_{res} = the resuspension rate parameter (g m^{-2} d^{-1})

τ_{flow} = ½ ρ_w c_f U_b^2

$\tau_{wave} = ½\ \rho_w\ f_w\ U_{orb}^2$

f_w = *a wave friction coefficient according to Swart (1974)*

$$DMS = IM1S + IM2S + POCS$$

Burial

$$bur_{POX_S} = \frac{b*POXS}{Z}$$

$$bur_{BSi_S} = \frac{b*BSiS}{Z}$$

A2.3. Descriptions of symbols

Symbol	Description	unit
	State variables	
NO_3	Nitrate	gN m^{-3}
NH_{4a}	ammonium	gN m^{-3}
PO_4	orthophosphate	gP m^{-3}
Si	dissolved silicate	gSi m^{-3}
O_2	dissolved oxygen	gO_2 m^{-3}
ALG_i	algae species / phenotypes	gC m^{-3}
POC	particulate organic carbon	gC m^{-3}
PON	particulate organic nitrogen	gN m^{-3}
POP	particulate organic phosphorus	gP m^{-3}
BSi	biogenic silica	gSi m^{-3}
DOC	dissolved organic carbon	gC m^{-3}
DON	dissolved organic nitrogen	gN m^{-3}
DOP	dissolved organic phosphorus	gP m^{-3}
POC_S	particulate organic carbon in the sediment	gC m^{-2}
PON_S	particulate organic nitrogen in the sediment	gN m^{-2}
POP_S	particulate organic phosphorus in the sediment	gP m^{-2}
BSi_S	biogenic silica in the sediment	gSi m^{-2}
SAL	Salinity	ppt
	Fluxes	
sed	settling	gX m^{-3} d^{-1}
res	Resuspension	gX m^{-3} d^{-1}
mrt	phytoplankton mortality	gC m^{-3} d^{-1}
gro	net phytoplankton growth	gC m^{-3} d^{-1}
mor	formation of dead organic matter by phytoplankton mortality	gX m^{-3} d^{-1}
upt	uptake of nutrients by phytoplankton growth	gX m^{-3} d^{-1}
dec	decomposition of dead particulate organic matter	gX m^{-3} d^{-1}
dis	dissolution of biogenic silica	gSi m^{-3} d^{-1}

Symbol	Description	unit
bur	burial	gX m^{-3} d^{-1}
den	denitrification	gN m^{-3} d^{-1}
nit	Nitrification	gN m^{-3} d^{-1}
rea	Reaeration	gO_2 m^{-3} d^{-1}
	Explanation of symbols	
Δt	time step for processes (different than for transport)	d
$ALG_{i,new}$	concentration of algae type *i* at the end of the time step	gC m^{-3}
b	burial rate	d^{-1}
b_{pocdoc}	fraction of POX converted to DOX	-
Cl	chloride concentration	g m^{-3}
DMS	solid matter in top sediment layer	g m^{-2}
e_{ALGi}	specific extinction of algae type *i*	m^2 gC^{-1}
e_{DOC}	specific extinction of dissolved organic matter	m^2 gC^{-1}
e_{POC}	specific extinction of particulate dead organic matter	m^2 gC^{-1}
e_{IM}	specific extinction of inorganic suspended matter	m^2 g^{-1}
f_{am}	fraction ammonium in nitrogen uptake	-
f_{aut}	autolysis fraction of mortality	-
f_{nut}	function for relative nutrient availability	-
f_{table}	tabulated function relating k_d to growth efficiency, converted from the tabulated function of growth efficiency and light	m^{-1}
$f_{T,pr}$	temperature function for process pr = dec, den, nit	-
F_{res}	total resuspension flux	g m^{-2} d^{-1}
IM	(suspended) inorganic matter concentration	gDM m^{-3}
IM1S	fine inorganic particles in top sediment layer	g m^{-2}
IM2S	coarse inorganic particles in top sediment layer	g m^{-2}
k_{ALG}	total extinction due to phytoplankton	m^{-1}
k_b	background extinction	m^{-1}
k_d	total extinction coefficient	m^{-1}
k_{decDOC}	decomposition rate for DOC, DON, DOP at 20°C	d^{-1}
$k_{decL,\ POC}$	minimum decomposition rate for POC at 20°C	d^{-1}
$k_{decL,\ PON}$	minimum decomposition rate for PON at 20°C	d^{-1}
$k_{decL,\ POP}$	minimum decomposition rate for POP at 20°C	d^{-1}
$k_{dec,POCS}$	decomposition rate for POC in sediment at 20 °C	d^{-1}
$k_{dec,PONS}$	decomposition rate for PON in sediment at 20 °C	d^{-1}
$k_{dec,POPS}$	decomposition rate for POP in sediment at 20 °C	d^{-1}
$k_{decH,\ POC}$	maximum decomposition rate for POC at 20°C	d^{-1}
$k_{decH,\ PON}$	maximum decomposition rate for PON at 20°C	d^{-1}
$k_{decH,\ POP}$	maximum decomposition rate for POP at 20°C	d^{-1}
k_{den}	denitrification rate	m d^{-1}
$k_{dis,\ BSi}$	dissolution rate for BSi at 20°C	d^{-1}
$k_{dis,BSiS}$	dissolution rate for BSi in sediment at 20 °C	d^{-1}
k_{DOM}	extinction due to dissolved organic matter	m^{-1}

Symbol	Description	unit
$k_{max,I}$	maximum extinction where the net growth of algae type *i* is positive; above this level self shading limits growth	m^{-1}
$k_{min,I}$	minimum extinction where the net growth of algae type *i* is positive; below this level photo-inhibition limits growth	m^{-1}
k_{nit}	nitrification rate	d^{-1}
k_{POM}	extinction of dead particulate organic matter	m^{-1}
k_{rea}	reaeration rate	d^{-1}
k_{SPM}	extinction of inorganic suspended matter	m^{-1}
kt_{dec}	temperature coefficient for decomposition of POX and POXS, except for opal silicate in sediment	-
kt_{den}	temperature coefficient for denitrification	-
kt_{dis}	temperature coefficient for dissolution of opal silicate	-
$kt_{m,i}$	temperature coefficient for mortality of algae type *i*	-
kt_{nit}	temperature coefficient for nitrification	-
$kt_{p,i}$	temperature coefficient for phytoplankton growth	°C
$kt_{r,i}$	temperature coefficient for phytoplankton respiration	-
le_{cr}	critical light efficiency where phytoplankton growth just balances losses	-
le_i	growth efficiency of algae type *i*, tabulated function of light	-
$m_{i,0}$	mortality rate for algae type *i* at 0 °C	d^{-1}
$m_{G,20}$	maximum mortality rate of grazers at 20 °C	d^{-1}
m_i	mortality rate for algae type *i*	d^{-1}
n	number of algae types in calculation	-
$O_{2,eq}$	saturation concentration of oxygen	$gO_2\ m^{-3}$
$p_{i,0}$	maximal net growth rate of algae type *i* at 0 °C	d^{-1}
pg_i	maximal gross growth rate algae type *i*	d^{-1}
p_i	maximal net growth rate for algae type *i*	d^{-1}
$r_{i,0}$	maintenance respiration rate for algae type *i* at 0 °C	d^{-1}
r_i	maintenance respiration rate for algae type *i*	d^{-1}
Si_{eq}	saturation concentration of Si	$gSi\ m^{-3}$
sl_N	lower limit stoichiometric constant PON	$gN\ gC^{-1}$
sl_P	lower limit stoichiometric constant POP	$gP\ gC^{-1}$
sl_{Si}	lower limit stoichiometric constant POSi	$gSi\ gC^{-1}$
s_{NO}	oxygen nitrogen ratio in NO_3	$gO_2\ gN^{-1}$
s_O	oxygen carbon ratio in detritus	$gO_2\ gC^{-1}$
su_N	upper limit stoichiometric constant PON	$gN\ gC^{-1}$
su_P	upper limit stoichiometric constant POP	$gP\ gC^{-1}$
su_{Si}	upper limit stoichiometric constant POSi	$gSi\ gC^{-1}$
$s_{X,i}$	stochiometry of nutrient X in algae type *i*	gX/gC
τ_{flow}	shear stress exerted by currents	Pa
τ_{waves}	shear stress exerted by waves	Pa
$\tau_{cr,res}$	critical shear stress for resuspension	Pa
T	water temperature	°C

Symbol	Description	unit
v_{ALGi}	settling velocity of algae type *i*	m d^{-1}
v_{BSi}	settling velocity of biogenic silica	m d^{-1}
v_{POX}	settling velocity of particulate dead organic matter	m d^{-1}
W	wind velocity	m s^{-1}
Z_{res}	zero order resuspension parameter	g m^{-2} d^{-1}
Z	thickness of above sediment water layer	m

A2.4. Parameter values in the BLOOM algal module

Table A2.1 Parameter values used in BLOOM to describe the modeled algae types (from Blauw et al., 2009).

ALG_i	e_{ALGi}	$s_{N,i}$	$s_{P,i}$	$s_{Si,i}$	$s_{Chl,i}$	$p_{i,0}$	$kt_{p,i}$	$m_{i,0}$	$kt_{m,i}$	v_{ALGi}
diat-E	0.2400	0.2170	0.0315	0.4470	0.0200	0.0830	-1.75	0.1400	1.0720	0.5
diat-N	0.2100	0.1960	0.0299	0.2830	0.0100	0.0660	-2.00	0.1600	1.0850	1.0
diat-P	0.2100	0.2060	0.0284	0.1520	0.0100	0.0660	-2.00	0.1600	1.0850	1.0
flag-E	0.2500	0.2000	0.0200	0.0	0.0140	0.0900	-1.00	0.1400	1.0720	0.0
flag-N	0.2250	0.1800	0.0190	0.0	0.0070	0.0750	-1.00	0.1600	1.0850	0.5
flag-P	0.2250	0.1900	0.0180	0.0	0.0070	0.0750	-1.00	0.1600	1.0850	0.5
dino-E	0.2000	0.1630	0.0168	0.0	0.0140	0.1320	5.50	0.1500	1.0720	0.0
dino-N	0.1750	0.1460	0.0159	0.0	0.0070	0.1130	4.75	0.1600	1.0850	0.0
dino-P	0.1750	0.1540	0.0151	0.0	0.0070	0.1120	4.75	0.1600	1.0850	0.0
Phaeo-E	0.4500	0.1880	0.0225	0.0	0.0140	0.0840	-1.00	0.1400	1.0720	0.0
Phaeo-N	0.4125	0.1690	0.0214	0.0	0.0070	0.0780	-1.00	0.1600	1.0850	0.5
Phaeo-P	0.4125	0.1780	0.0203	0.0	0.0070	0.0780	-1.00	0.1600	1.0850	0.5

A2.5. Process library user manual

Additional details about the water quality processes equations can be found in Deltares, 2020.

Appendix A3. Outfall discharge locations

Coordinates (latitude, longitude) of the 55 effluent risers (R1-R55).

STAT_ID	TARGET_LAT	TARGET_LON	AVG_WATER_DEPTH (m)
R55	42.384312	-70.803795	32.8
R54	42.384399	-70.803322	33.14
R53	42.384483	-70.802895	33.08
R52	42.384567	-70.802444	33.29
R51	42.384655	-70.802002	33.47
R50	42.384743	-70.801544	33.5
R49	42.384827	-70.801109	33.69
R48	42.384914	-70.800659	33.87
R47	42.384995	-70.800224	33.84
R46	42.385082	-70.799774	33.96
R45	42.38517	-70.799332	34.11
R44	42.385265	-70.798843	34.05
R43	42.385342	-70.798439	34.08
R42	42.385426	-70.797989	34.05
R41	42.385517	-70.797546	34.02
R40	42.385597	-70.797096	33.81
R39	42.385685	-70.796654	33.6
R38	42.385769	-70.796204	33.26
R37	42.385857	-70.795761	33.17
R36	42.385944	-70.795311	33.05
R35	42.386017	-70.794876	32.83
R34	42.38612	-70.794418	32.83
R33	42.3862	-70.793976	32.92
R32	42.386284	-70.793526	32.86
R31	42.386372	-70.793083	33.14
R30	42.386456	-70.792641	33.02
R29	42.386543	-70.792191	33.41
R28	42.386627	-70.79174	33.32
R27	42.386715	-70.791298	33.41
R26	42.386795	-70.790848	33.56
R25	42.386883	-70.790405	33.78
R24	42.386971	-70.789963	33.87
R23	42.387054	-70.78952	34.05

R22	42.387138	-70.78907	34.24
R21	42.387226	-70.78862	34.33
R20	42.387314	-70.78817	34.57
R19	42.387402	-70.787727	34.57
R18	42.387486	-70.787285	34.81
R17	42.387573	-70.786842	34.88
R16	42.387657	-70.786392	34.88
R15	42.387756	-70.785927	34.88
R14	42.387825	-70.785461	34.84
R13	42.387909	-70.785057	34.88
R12	42.387989	-70.784592	34.88
R11	42.388084	-70.784164	34.72
R10	42.388168	-70.783714	35.03
R09	42.388256	-70.783272	35.03
R08	42.388344	-70.782814	35.03
R07	42.388435	-70.782417	35.09
R06	42.388512	-70.781929	35.12
R05	42.388599	-70.781494	35.03
R04	42.388683	-70.781036	35.06
R03	42.388771	-70.780586	35.12
R02	42.388855	-70.780121	35.15
R01	42.388683	-70.78009	35.15